Sedimentology (2006) **53,** 971–1013 doi: 10.1111/j.1365-3091.2006.00795.x

Tidal-channel deposits on a delta plain from the Upper Miocene Nauta Formation, Marañón Foreland Sub-basin, Peru

LUISA A. REBATA-H.*, MURRAY K. GINGRAS†, MATTI E. RÄSÄNEN* and MAIRA BARBERI‡

**Department of Geology, University of Turku, 20014 Turku, Finland (E-mail: luireb@utu.fi)*

†Department of Earth & Atmospheric Sciences, University of Alberta, Edmonton, Alberta, Canada T6G 2E3

‡Laboratory of Palaeoecology, Centre of Biological Studies and Research, Catholic University of Goiás, CP. 86 – Goiania-GO, 74605-010, Brazil

ABSTRACT

Miocene siliciclastic sediments of the Marañón Foreland Sub-basin in Peru record the sedimentary response to regional marine incursions into Amazonia. Contrary to previous interpretations, the Late Miocene Nauta Formation provides evidence of the last known marine incursion before the current Amazonia river basin became established. Sedimentological, ichnological and palynological data from well-exposed outcrops along a *ca* 100 km road transect suggest that the Nauta Formation represents a shallow, marginal-marine channel complex dominated by tidal channels developed in the inactive, brackish-water portions of a delta plain. The main facies associations are: FA1 – slightly bioturbated mud-draped trough cross-stratified sand; FA2 – locally, pervasively bioturbated inclined heterolithic stratification (IHS); and FA3 – moderately bioturbated horizontally bedded sand–mud couplets. These identify subtidal compound dunes, tidal point bars and shallow subtidal to intertidal flats, respectively. Bi-seasonal depositional cycles are ascribed to the abundant metre- to decimetre-scale sand–mud couplets that are found mainly in the IHS association: semi-monthly to daily tidal rhythmicity is inferred from centimetre- and millimetre-scale couplets in the mud-dominated parts of the decimetre-scale couplets. The ichnology of the deposits is consistent with brackish depositional conditions; the presence of *Laminites*, a variant of *Scolicia*, attests to episodic normal marine conditions. Trace fossil suites are assigned to the *Skolithos*, *Cruziana* and mixed *Skolithos–Cruziana* ichnofacies. Pollen assemblages related to mangrove environments (e.g. *Retitricolporites* sp., *Zonocostites* sp., *Psilatricolporites maculosus*, *Retitricolpites simplex*) support a brackish-water setting. Uplift of the Mérida Andes to the North and the consequent closure of the Proto-Caribbean connection, and the onset of the transcontinental Amazon drainage, constrain the deposition of the Nauta sediments with around 10 to 8 Ma, probably contemporaneous to similar marine incursions identified in the Cuenca (Ecuador), Acre (Brazil) and Madre de Dios (Southern Peru) (sub)basins, and along the Chaco-Paranan corridor across Bolivia, Paraguay and Argentina.

Keywords Amazonia Peru, delta plain, inclined heterolithic stratification, Late Miocene, Marañón foreland sub-basin, Nauta Formation.

INTRODUCTION

The palaeogeography of north-western Amazonia during the Neogene is still poorly understood, despite a long history of research, mainly palaeontological and palynological in scope (see Nuttall, 1990; Hoorn, 1993a,b, 1994a,b,c; Hoorn *et al.*, 1995; Räsänen *et al.*, 1995; Webb, 1995; Wesse-

lingh *et al.*, 2002; Vonhof *et al.*, 2003; Hoorn & Vonhof, 2006). This is not only because of the difficult access afforded by the Amazonian rainforest, but also reflects the complex geotectonic regime in South America (see Fig. 1). During the Late Cretaceous, a large foreland basin developed between the Precambrian Amazon Craton to the east, comprising mainly the Guyana and Brazilian shields, and an active continental magmatic arc represented by the Andean Belt to the west. Uplift of the Andes commenced *ca* 90 Ma, as a result of the eastward subduction of the oceanic Nazca Plate beneath the South American Continental Plate (Jordan *et al.*, 1983).

The modern South American foreland basin system contains a thick Cenozoic succession derived from the Andes (Horton & DeCelles, 1997; Sánchez-F. *et al.*, 1999). The basin fill is 3–7 km thick in the west, declining to 0·5–1·5 km in the east. It can be divided into three major basin complexes: the southern Caribbean, the Amazonian and the southern South American foreland basins (Horton & DeCelles, 1997; Jacques, 2003a,b; Roddaz *et al.*, 2005; Fig. 1). The basins are further compartmentalized into sub-basins by structural highs or basement arches (Gil, 2001; Jacques, 2003a,b; Roddaz *et al.*, 2005). The Oriente Basin, the largest of the Amazonian basins (cf. Jacques, 2003a), covers the Putumayo sub-basin in south-western Colombia, the Napo sub-basin in eastern Ecuador, the Marañón (also referred to as Pastaza-Marañón) sub-basin in north-eastern Peru and the Acre sub-basin in western Brazil (Fig. 2).

The study reported in this paper focuses on the south-eastern margin of the Marañón sub-basin where foreland basin sedimentation commenced during the Late Oligocene–Early Miocene (Sánchez-F. *et al.*, 1999). Tectonically induced subsidence of the South American foreland basin was accompanied by several marine incursions through up to six possible gateways or portals (see e.g. Nuttall, 1990; Boltovskoy, 1991; Hoorn, 1993a,b, 1994a,b,c; Marshall *et al.*, 1993; Hoorn *et al.*, 1995; Räsänen *et al.*, 1995, 1998; Webb, 1995; Lundberg *et al.*, 1998; Vonhof *et al.*, 1998; Marengo, 2000; Rossetti, 2001; Gingras *et al.*, 2002a; Rossetti *et al.*, 2005; portals 1–6 in Fig. 1). It has been suggested that an inland brackish- to freshwater basin in northern South America included intermittent connections with the Proto-Caribbean Sea, and the Pacific and Atlantic Oceans through those portals (Fig. 1). Previous studies have identified three major transgressive pulses during the Miocene, each with different geographical extents (Fig. 1). The first was the Pirabas/Barreiras transgression (henceforth, the Pirabas/Barreiras system, Fig. 1), which occurred during the Early to Middle Miocene along what is now the Amazon river axis (Rossetti, 2001; Rossetti *et al.*, 2005; see Fig. 1, portal 4). The second was the Pebas transgression covering the north-western region of Amazonia (henceforth, the Pebas system; Fig. 1), which spanned from the late Early until the early Late Miocene (see Nuttall, 1990; Hoorn, 1993a; Hoorn *et al.*, 1995; Räsänen *et al.*, 1995; Wesselingh *et al.*, 2002 and references therein; see Fig. 1, portals 1, 2). Recent data from Brazilian Western Amazonia do not support a connection between the Pirabas/Barreiras and the Pebas systems (Rossetti *et al.*, 2005). Finally, there was the Paranan/Entrerriense transgression (henceforth, the Paranan/Entrerriense system; Fig. 1), which occurred during the Middle to Late Miocene (Marshall *et al.*, 1993; Marengo, 2000; see Fig. 1, portal 5). Two minor transgressions have also been suggested. One took place through portal 3 during the Middle to Late Miocene through the Maturín Basin (henceforth, the Maturín system) along what is now the Orinoco river axis, based on documentation by Hoorn (1994c) from the Apaporis area (Fig. 1, AA; see also Lundberg *et al.*, 1998; Vonhof *et al.*, 1998). The

Fig. 1. Map of South America showing major tectono-sedimentary elements (the Andes, foreland basins/sub-basins and shields), Miocene gaps or portals (1–6) and the extent of marine incursions during the Middle to Late Miocene (map modified from Jacques, 2003a,b; northernmost basins from Díaz de Gamero, 1996; portals and extent of incursions based on Nuttall, 1990; Hoorn, 1994c; Hoorn *et al.*, 1995; Räsänen *et al.*, 1995; Vonhof *et al.*, 1998; Steinmann *et al.*, 1999; Wesselingh *et al.*, 2002). A black circle indicates the location of the study area. eVB, Eastern Venezuela Basin; FB, Falcon Basin; MB, Maracaibo Basin; LB, Llanos Basin; mMB, Middle Magdalena Valley Basin; uMB, Upper Magdalena Valley Basin; AA, Apaporis Area; OB, Oriente Basin; SB, Santiago Basin; HB, Huallaga Basin; UB, Ucayali Basin; AS, Acre Sub-basin; SoB, Solimões Basin; AB, Amazonas Basin; FAB, Foz do Amazonas Basin; MPB, Maranhao (Parnaiba) Basin; MDB, Madre de Dios Basin; BPB, Beni Plain Basin; SCB, Santa Cruz Basin; NWB, Northwest Basin; CB, Chaco Basin; PB, Paraná Basin. Note that the extension of transgressions formed different systems adjacent to the portals: the Pebas, ?Maturín, Pirabas/Barreiras, Paranan/Entrerriense and Cuenca systems.

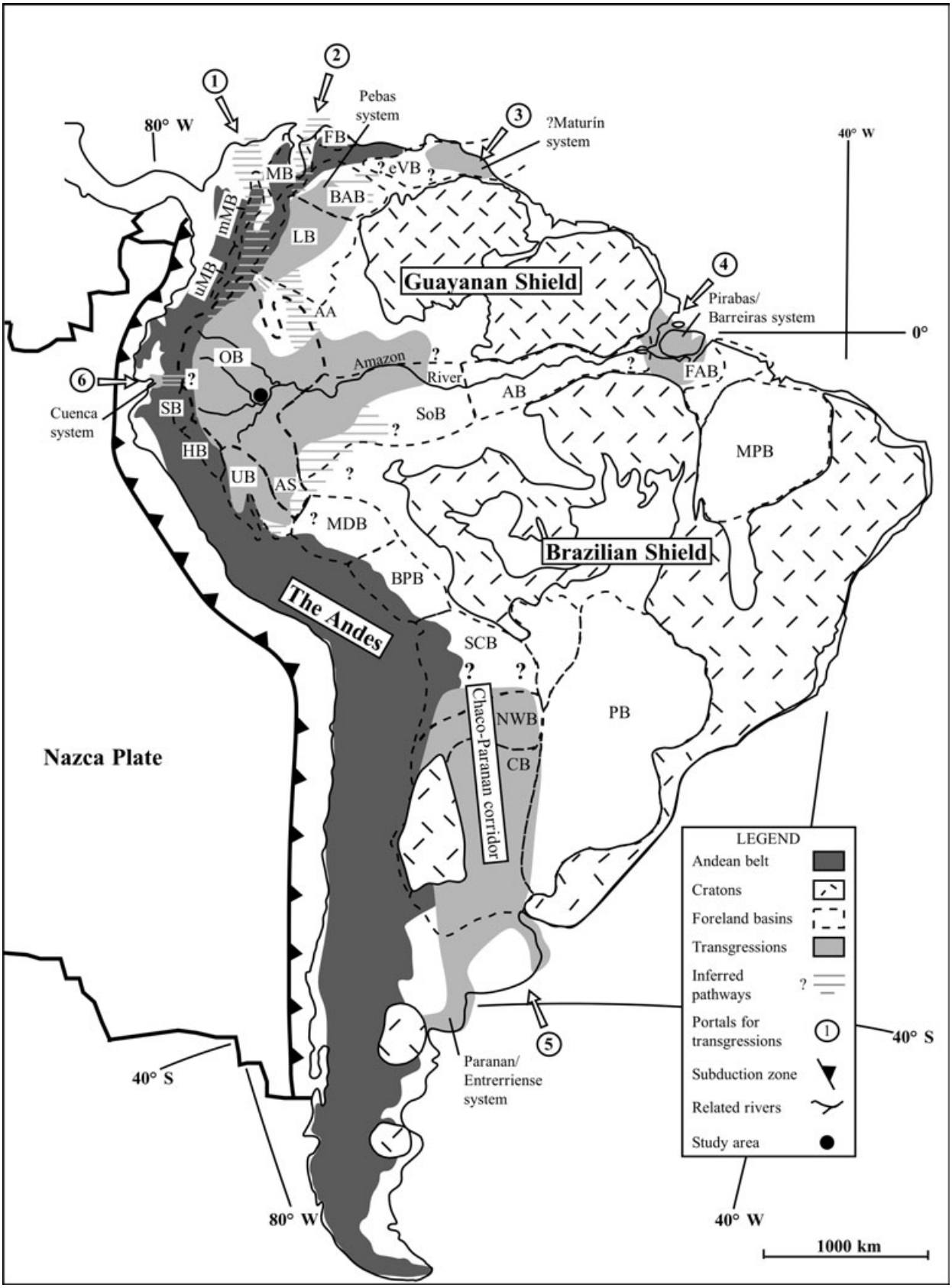

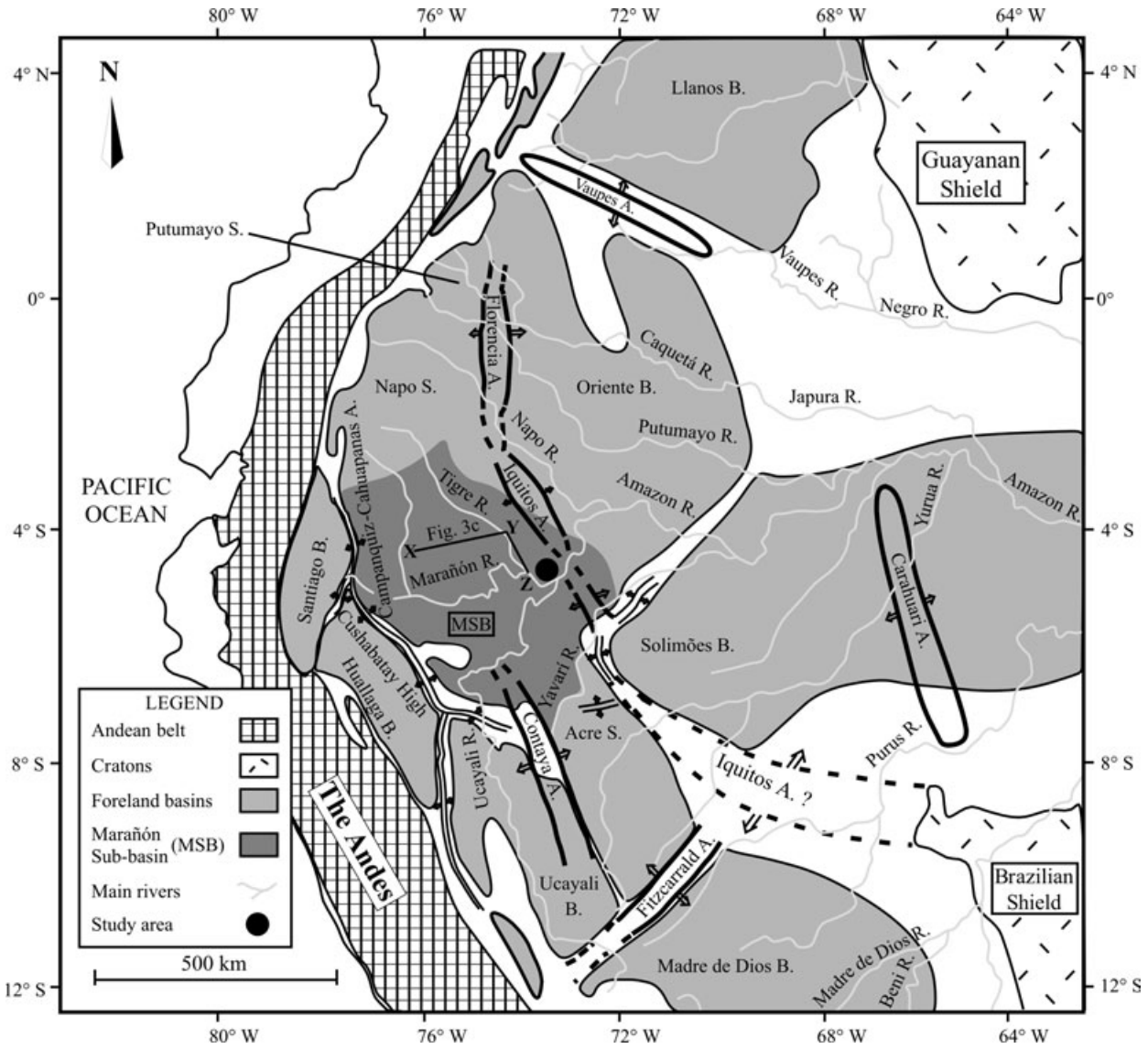

Fig. 2. Location of the Marañón Sub-basin (MSB) in Peru and position of major arches and highs. Notice the inferred (dashed lines) location of the Iquitos Arch (named Florencia Arch in Colombia). Compiled and modified from Martínez-V. *et al.* (1999), Sánchez-F. *et al.* (1999) and Jacques (2003a,b. Study area in black circle. A., arch; R., river; B., Basin; S., Sub-basin. Note location of line X–Y–Z (Fig. 3C).

other took place through portal 6 crossing the Cuenca area of Ecuador in the Early to Late Miocene (henceforth, the Cuenca system; cf. the Pacific Coastal Stage of Steinmann *et al.*, 1999; see also Nuttall, 1990; Hungerbühler *et al.*, 2002; Wesselingh *et al.*, 2002; Fig. 1). This transgression may have reached the Oriente Basin. The Paranan/Entrerriense, Maturín and Cuenca systems may have been connected to the Pebas system, although there is still no conclusive evidence for this (see Räsänen *et al.*, 1995; Webb, 1995; Díaz de Gamero, 1996; Lundberg *et al.*, 1998; Marengo, 2000; Mörner *et al.*, 2001; Gingras *et al.*, 2002a; Martínez & del Río, 2002; Wesselingh *et al.*, 2002; Boeger & Kritsky, 2003; Vonhof *et al.*, 2003; Hoorn & Vonhof, 2006; Hulka *et al.*, 2006).

In the Marañón sub-basin in Peru, evidence for marine incursions is recorded in the palynologically dated late Early to early Late Miocene Pebas Formation with transgression reportedly from the North (e.g. Hoorn, 1993a,b, 1994a,b,c; Räsänen *et al.*, 1995, 1998; Vonhof *et al.*, 1998, 2003; Gingras *et al.*, 2002b; Fig. 1). However, the depositional setting of the Pebas Formation is still under debate. Three settings have been proposed: (i) an epicontinental embayment with a sustained connection to the sea (e.g. Räsänen *et al.*, 1995,

1998); (ii) a long-lived lake with an ephemeral connection to the sea (Wesselingh *et al.*, 2002; Vonhof *et al.*, 2003); or (iii) an inland saline lake (e.g. Whatley *et al.*, 1998). Recently, the Nauta Formation has been distinguished as a succession of sediments overlying the Pebas outcrops in Peru (Rebata-H., 1997; Räsänen *et al.*, 1998; Martínez-V. *et al.*, 1999; Sánchez-F. *et al.*, 1999; Rebata-H. *et al.*, 2006). Preliminary data indicated that it was deposited in a tidally influenced environment (Rebata-H., 1997; Räsänen *et al.*, 1998). These findings are important because they imply that a marine incursion reached as far south as north-eastern Peru during the Late Miocene. This paper provides a detailed documentation of the sedimentology of the Nauta Formation, and shows that the system was tidally influenced, and that there was therefore a connection with the sea during the Late Miocene in Peruvian Amazonia. This last marine incursion places an important constraint on the timing of the onset of Amazon drainage. During the Late Miocene (*ca* 10–8 Ma), Andean tectonics and a global low eustatic level closed the connection between the internal embayments and the Caribbean Sea and the Pacific and Atlantic Oceans, and subsequently led to the establishment of the Amazon drainage system (Hoorn, 1993a,b, 1994a,b,c; Cooper *et al.*, 1995; Hoorn *et al.*, 1995; Guerrero, 1997; Lovejoy *et al.*, 1998; Lundberg *et al.*, 1998; Roddaz *et al.*, 2005).

GEOLOGICAL FRAMEWORK

The Marañón Sub-basin (MSB; Fig. 2) is an elongated basin (760 km long × 380 km wide) with a general NW–SE orientation, delimited to the west by the Campanquiz-Cahuapanas, Cushabatay and Contaya structural highs, and partly bounded to the east by the Iquitos Arch (referred to as the Florencia Arch in Colombia; Martínez-V. *et al.*, 1999; Sánchez-F. *et al.*, 1999; Gil, 2001; Jacques, 2003a,b; Roddaz *et al.*, 2005; Fig. 2). Major structures in the MSB run parallel to the Iquitos Arch in a NW–SE direction. Late Cretaceous to Tertiary deposits accumulated in the MSB, with the thickest fill preserved close to the Sub-Andean thrust front in the western margin of the basin, thinning to onlap the Iquitos Arch to the east (Martínez-V. *et al.*, 1999; Sánchez-F. *et al.*, 1999; Gil, 2001; Roddaz *et al.*, 2005; Fig. 3C).

The tectonic evolution of the MSB can be explained following the models for foreland basin systems established by DeCelles & Giles (1996) and Catuneanu *et al.* (1997) (see also Horton & DeCelles, 1997; Catuneanu *et al.*, 2000; Gil, 2001; Roddaz *et al.*, 2005). From the Palaeocene until the Late Miocene, sedimentation within the MSB mainly occurred in a distal foredeep setting during tectonic loading cycles, and in the foresag depozone during tectonic unloading cycles (Gil, 2001; Roddaz *et al.*, 2005). Marine incursions, like those being deposited in the Pebas Formation, took place during the unloading cycles, as during these periods subsidence dominated across most of the MSB (Gil, 2001). Towards the eastern margin of the MSB, sedimentation was in the backbulge depozone (Gil, 2001). Around 10–7 Ma, deformation along the Andean front resulted in a proximal foredeep setting in the MSB. During this time, the Iquitos Arch may have started to grow to become the forebulge of the sub-basin (Gil, 2001; Roddaz *et al.*, 2005). From the late Late Miocene onwards, the Iquitos Arch acted as an intermittently uplifted forebulge to the retroarc Andean foreland basin system (Roddaz *et al.*, 2005).

Miocene outcrops within the MSB are represented by siliciclastic sediments of the Pebas and Nauta formations in north-eastern Peru (Fig. 3A). The Pebas Formation overlies the Oligocene–Miocene Chambira Formation (equivalent to the Ramón Formation in Brazil), which is about 900 m thick in the sub-surface and consists of red mudstones interstratified with reddish brown siltstones and reddish yellow sandstones, anhydrite and gypsum (cf. Sánchez-F. *et al.*, 1999, their fig. 4.1; Fig. 3C). The Pebas Formation is exposed only in the north-east corner of the study area (in the vicinity of the Iquitos Arch; Sánchez-F. *et al.*, 1999; Figs 2 and 3A), where it shows a maximum thickness of about 9 m in outcrops, though regionally it may reach 18–20 m, and around 250 m in the sub-surface (Sánchez-F. *et al.*, 1999, their fig. 4.1; Table 1). The Pebas Formation comprises bluish-grey mud, fine-grained sand, lignite layers and organic muds (see e.g. Hoorn, 1993a,b, 1994b,c; Räsänen *et al.*, 1998; Sánchez-F. *et al.*, 1999). In the study area, the majority of exposures of the Pebas beds are sub-horizontal, with a regional dip of about 1–5° (Sánchez-F. *et al.*, 1999) towards the SW. An abundant fossil molluscan fauna is present, although the molluscan content decreases upwards in the formation (Hoorn, 1994c; Räsänen *et al.*, 1998; Vonhof *et al.*, 1998; Rebata-H. *et al.*, 2006). The molluscs mainly indicate freshwater conditions (Vonhof *et al.*, 1998, 2003; Wesselingh *et al.*, 2002), although molluscs tolerant to brackish water have

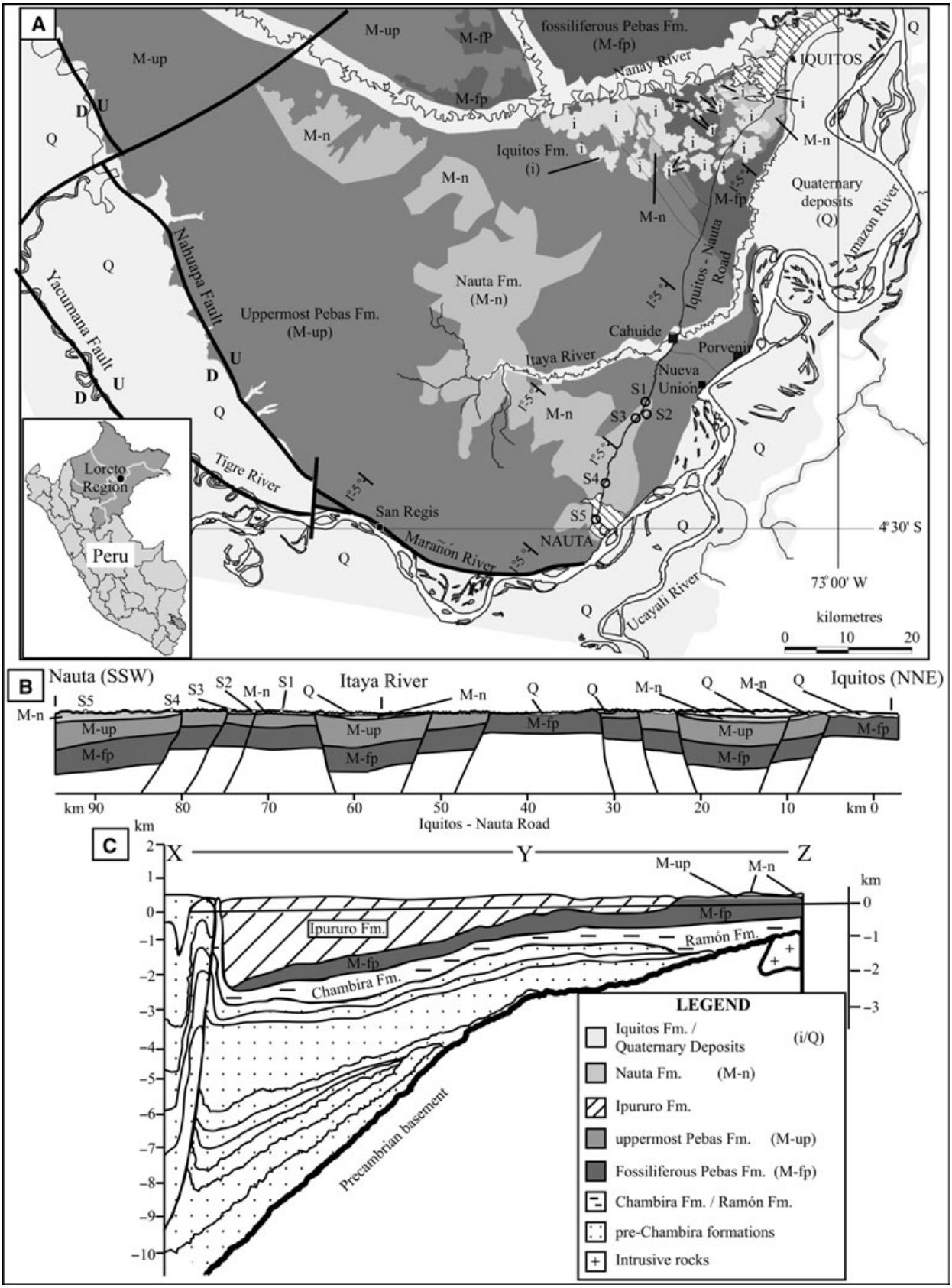
A
M-up
M-fP
fossiliferous Pebas Fm.
(M-fp)
Nanay River
IQUITOS
Q
M-fp
M-n
Iquitos Fm.
(i)
Quaternary
deposits
(Q)
Amazon River
Iquitos - Nauta
Road
Nahuapa Fault
Yacumana Fault
Nauta Fm.
(M-n)
Uppermost Pebas Fm.
(M-up)
Cahuide
Porvenir
Itaya River
Nueva
Unión
S1
S2
S3
S4
S5
Loreto
Region
Peru
Tigre River
San Regis
Marañón River
NAUTA
4°30' S
73°00' W
Ucayali River
kilometres
0 10 20
B
Nauta (SSW)
Itaya River
Iquitos (NNE)
km 90 80 70 60 50 40 30 20 10 km 0
Iquitos - Nauta Road
C
km
X
Y
Z
Ipururo Fm.
Ramón Fm.
Chambira Fm.
Precambrian basement
LEGEND
Iquitos Fm. /
Quaternary Deposits (i/Q)
Nauta Fm. (M-n)
Ipururo Fm.
uppermost Pebas Fm. (M-up)
Fossiliferous Pebas Fm. (M-fp)
Chambira Fm. / Ramón Fm.
pre-Chambira formations
Intrusive rocks

Table 1. Miocene stratigraphic framework for the study area. Notice that the division of the Pebas Formation into lowermost, lower, middle, upper and uppermost is an informal division based on the position of the Pebas beds within the Miocene palynological and molluscan schemes developed by Hoorn (1993a, 1994b) and Wesselingh *et al.* (2002), respectively.

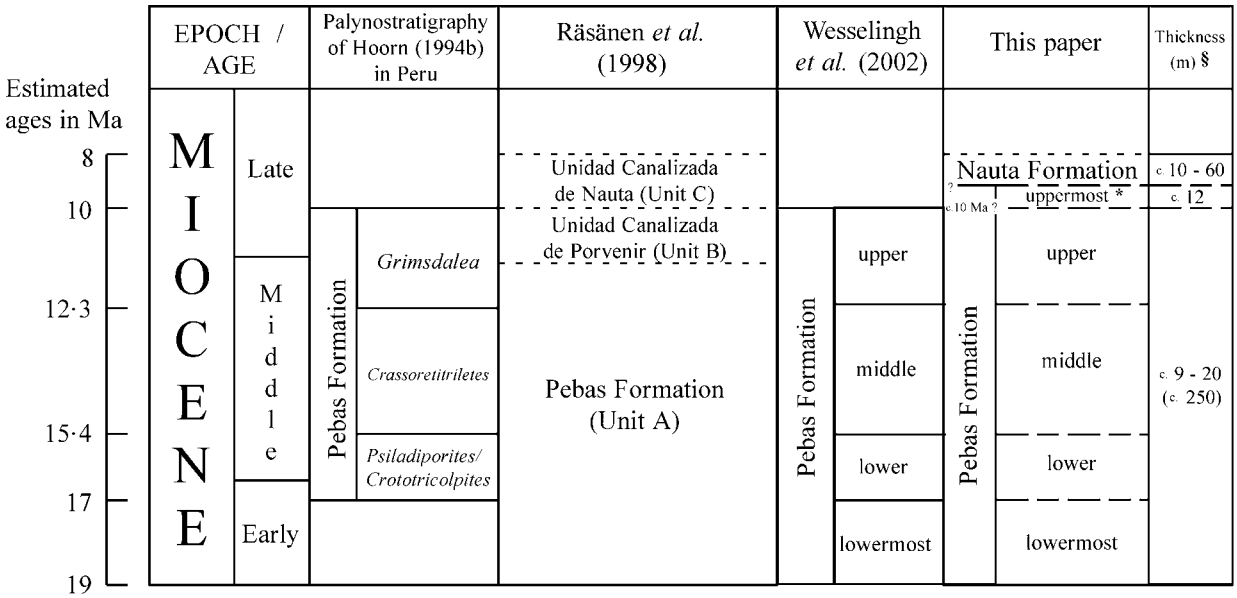

* Palynological content correlatable with the *Fenestrites* Sub-zone of Lorente (1986) and *Echitricolporites spinosus* Zone of Germeraad *et al.* (1968) and Muller *et al.* (1987), suggesting a Late Miocene age (Rebata-H. *et al.*, in press).
§ Local to regional thickness of the outcropping formations (modified after Martínez-V. *et al.*, 1999; Sánchez-F. *et al.*, 1999). The 250 m value for the Pebas Formation indicates sub-surface measurements from the closest drilled wells in the study area (Sánchez-F. *et al.*, 1999).

been also described, especially towards the top of the formation (Hoorn, 1994c). Controversially, trace fossil assemblages indicate brackish-water depositional conditions (Gingras *et al.*, 2002b). The Pebas Formation has been divided into three palynological zones by Hoorn (1994b,c) and four informal units by Wesselingh *et al.* (2002) based on its fossil molluscan fauna (Table 1). The Pebas Formation is equivalent to the Solimões Formation in Brazil (Maia *et al.*, 1977; Hoorn, 1993b, 1994c), the Curaray Formation in Ecuador (Gil, 2001; see also Wesselingh *et al.*, 2002), and the 'Pebas' and 'La Tagua Beds' in Colombia (Hoorn, 1994b,c; see also Wesselingh *et al.*, 2002).

In the study area, the top of the Pebas Formation is characterized by a mollusc-barren vertical transition to the Nauta Formation (Räsänen *et al.*, 1998; Rebata-H. *et al.*, 2006). This interval, over *ca* 12 m thick, has been assigned to the uppermost parts of the Pebas Formation (Rebata-H. *et al.*, 2006; Table 1). Outcrops of the uppermost parts of the Pebas Formation are exposed in the central part of the study area and to the south-west where they are in fault contact with Quaternary deposits running parallel to the Tigre and Marañón rivers (Räsänen *et al.*, 1998; Martínez-V. *et al.*, 1999; Sánchez-F. *et al.*, 1999; Rebata-H. *et al.*, 2006; Fig. 3A). Recent pollen data gathered from the uppermost Pebas beds by Rebata-H. *et al.* (2006) are correlatable with Late Miocene palynological zones (Table 1).

The Nauta Formation rests conformably on top of the Pebas Formation (cf., Räsänen *et al.*, 1998;

Fig. 3. (A) Geological map of the Iquitos–Nauta region. Notice location of studied sections (S1–S5) along the Iquitos–Nauta Road. Inset shows the location of the study area in the Loreto Region, Peru (black circle). Modified from Räsänen *et al.* (1998), Martínez-V. *et al.* (1999) and Sánchez-F. *et al.* (1999). (B) Schematic SSW–NNE cross-section along the Iquitos–Nauta Road showing the NW–SE normal fault system bounding horst and graben structures (after Sánchez-F. *et al.*, 1999). (C) Schematic west–east section across the study area. See location of line X–Y–Z in Fig. 2. Note that the Marañón foreland sub-basin fill is *ca* 11 km thick close to the Sub-Andean thrust fold front and *ca* 1 km thick in the study area. Modified after Martínez-V. *et al.* (1999) and Sánchez-F. *et al.* (1999). Data from Perupetro S.A.

Rebata-H. *et al.*, 2006) and it extends laterally to the frontier with Ecuador (see Cerrón-Z. *et al.*, 1999). The regional dip of the Nauta Formation is inferred to follow the dip of the Pebas beds and it is generally *ca* 20–25 m thick (Sánchez-F. *et al.*, 1999) but locally up to 60 m (Martínez-V. *et al.*, 1999). It has not been reported from the sub-surface. The Nauta Formation crops out as a NW–SE elongated belt in the centre of the study area (Fig. 3A). Its stratotype (cf. Martínez-V. *et al.*, 1999) is well exposed along the Iquitos–Nauta Road, in between Nauta and the Itaya River (Fig. 3A; Rebata-H., 1997; Räsänen *et al.*, 1998; Rebata-H. *et al.*, 2006). Here, the Nauta Formation is represented by 8–13 m of bluish-grey to variegated heterolithic deposits of mud and fine-grained sand containing brackish-water to normal marine trace-fossil suites (Unit C of Räsänen *et al.*, 1998; see also Rebata-H., 1997; Rebata-H. *et al.*, 2006). Characteristic mud brecciated layers and an overall coarser grain size differentiate the Nauta from the Pebas deposits. The stratigraphic position (cf. Räsänen *et al.*, 1998; Rebata-H. *et al.*, 2006) and palynological data documented below for the Nauta stratotype (see below) suggest a Late Miocene age for this unit. Previous researchers have suggested that the Nauta Formation primarily accumulated as a fluvial deposit and that it is of Pliocene–Pleistocene age (e.g. Cerrón-L. *et al.*, 1999; Martínez-V. *et al.*, 1999; Sánchez-F. *et al.*, 1999). However, the integrated sedimentological, ichnological and palynological work described below suggests otherwise.

The Nauta Formation is unconformably overlain by the Pliocene to Pleistocene Iquitos Formation (thickness 12 m), a white, quartz-rich sand interpreted as a fluvial deposit (Räsänen *et al.*, 1998; Sánchez-F. *et al.*, 1999, their fig. 4.1). The Iquitos Formation is patchily exposed in the north-east corner of the study area, between the Nanay and Itaya rivers (see Fig. 3A for location).

MATERIAL AND METHODS

Study sites

The study area is located at the south-eastern margin of the Marañón Sub-basin flanking the Iquitos Arch (Fig. 2), where well preserved, up to 13 m high, unlithified outcrops of the Nauta Formation are continuously exposed along a 26 km stretch of the Iquitos–Nauta Road, close to Nauta, in the Loreto Region of Peru (Fig. 3A). Five representative outcrops (sections S1–S5; see Fig. 3A for location) were selected to document the facies architecture of the Nauta Formation. These span the range of features observed in the formation, and represent sections where the sedimentary structures are particularly well exposed (Fig. 4). The outcrops are identified by the distance in kilometres from Nauta. Because bedding in the Nauta Formation is almost subhorizontal, elevation differences of about 30 m along the road help to place the studied sections vertically within the formation. The lowermost levels are represented by sections 1 and 5, the central parts of the formation by sections S2 and S3, and the top of the formation by section 4 (Fig. 19).

Field methods

The facies architecture was documented by detailed sedimentological logging. Observations and measurements such as grain-size variation, mineralogical composition, physical and biogenic sedimentary structures [the size, distribution, strength of bioturbation (ichnofabric index) and types of trace fossil], and the orientation of major bounding surfaces and foresets of ripples and dunes were recorded. The ichnofabric index (i.i.) used varies from 1 to 5, with 20% increments for each class (i.e. i.i. equals 1 where bioturbation in the area examined ranges from 1% to 20%, i.i. equals 2 where bioturbation ranges from 21% to

Fig. 4. Selected pictures from the study area. (A) Panoramic view of section 5. Note organic-rich trough cross-bedded sand–mud couplets (FA1B) overlain by inclined heterolithic stratification (FA2). Person for scale in lower left corner. (B) Panoramic view of section 2. Note inclined heterolithic stratification (FA2A). Person for scale. (C) Trough cross-stratified sand (FA1A). Arrows identify mud drapes (M). Pen is *ca* 12 cm long. (D) Brecciated clay (FA2C) composed of tabular blocks. Blocks are either massive-appearing or laminated. Measuring tape extended 1 m. (E) Triplet/tetraplet rhythmites with tan sand, whitish mud, organic debris (O; in black) and elemental sulphur (S°; in yellow) laminae. Note pyrite nodules (Py). (F) Sand (in white) and mud (in red) rhythmites within IHS; Notice interpretation of neap (N) and spring (S), and ebb/flood (E/F) tidal cycles. (G) Soft sediment deformation including translated and rotated organic-rich laminated blocks formed by bluish grey mud and sand couplets (FA1B). Pen is *ca* 12 cm long. (H) Rip-up mud clasts (see arrows) with elongated shapes aligned along foresets within cross-stratified sand (FA1A). Pen is *ca* 12 cm long.

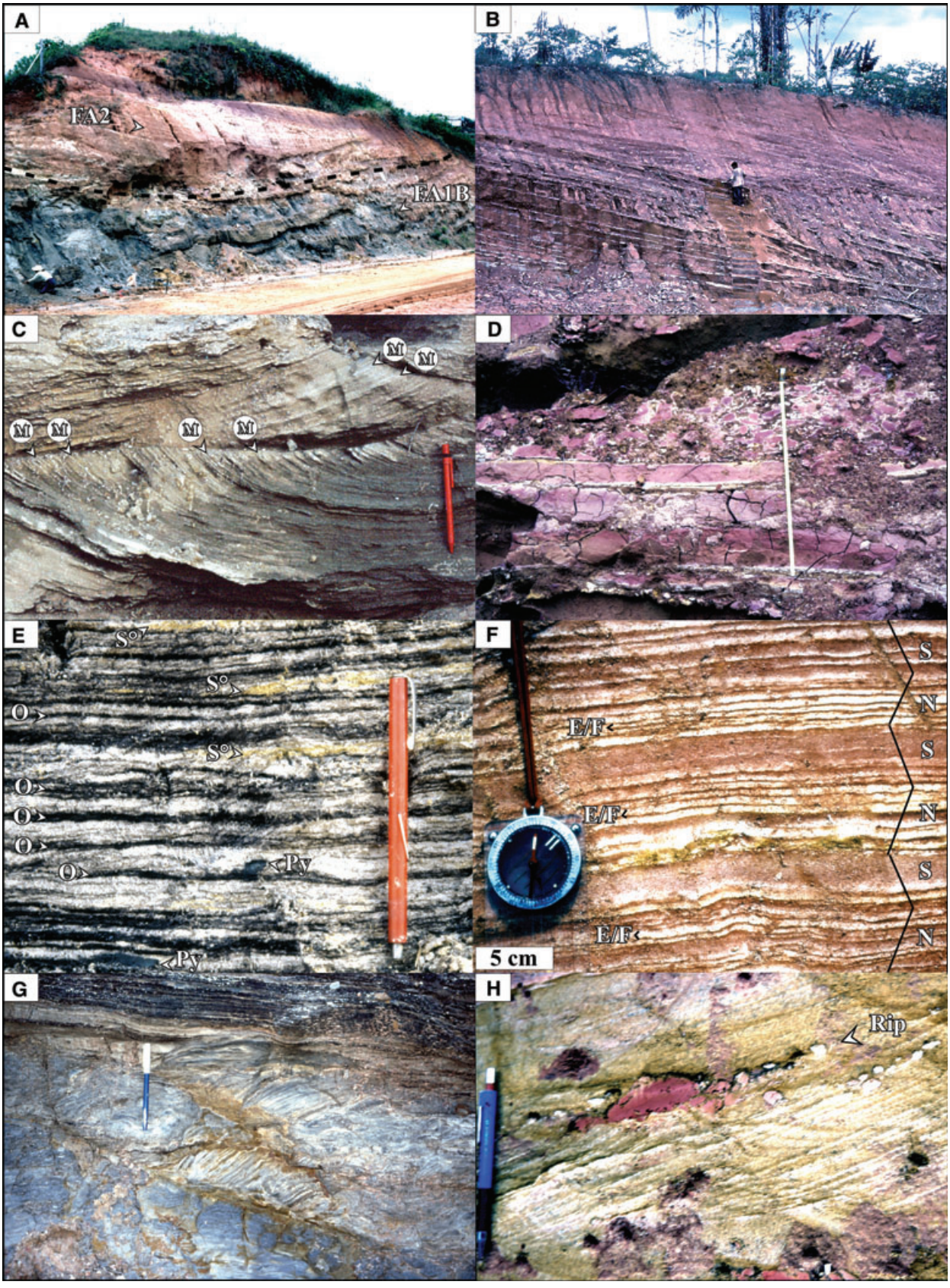
A
FA2
FA1B
B
C
M
M
M
M
M
M
D
E
S°
S°
O
S°
O
O
O
O
Py
Py
F
S
N
S
N
S
N
E/F
E/F
E/F
5 cm
G
H
Rip

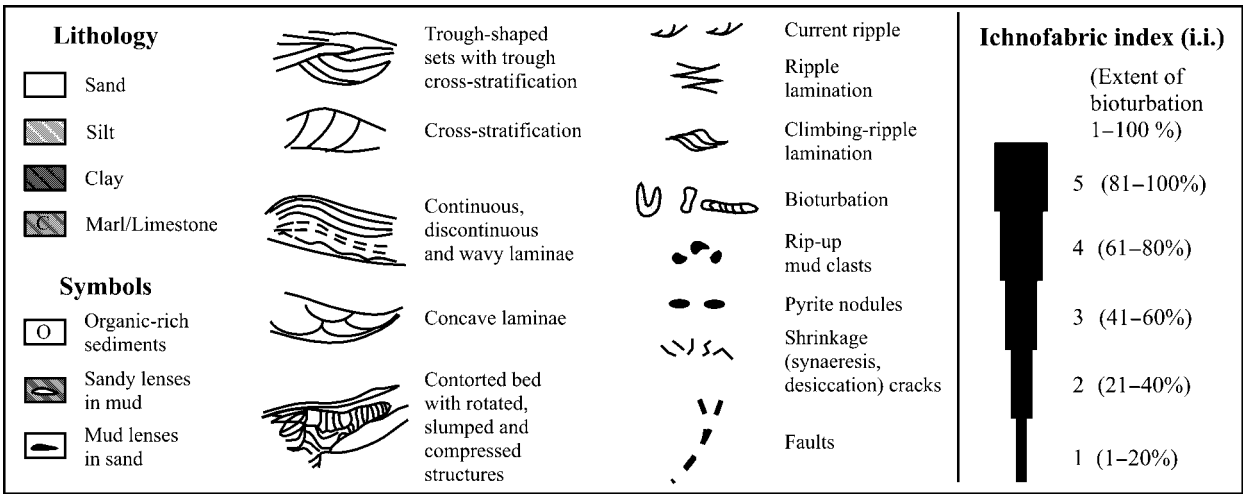

Fig. 5. Legend and symbols for Figs 6–16. Ichnofabric index (1 to 5) identifies extent of bioturbation in 20% increments (cf. Gingras *et al.*, 2002a,b).

40%, etc.; cf. Gingras *et al.*, 2002a,b; Fig. 5). The outcrops were also sampled for grain size and clay mineralogical analyses. In addition, several samples from organic-rich sediments (at sections 1 and 5) were collected for palynological study; however, fossil pollen was only found in one sample from organic-rich rhythmites in section 5 (FA1B; see results below). The length of the outcrops ranges from 49 to 114 m.

Laboratory methods

Grain size was quantified using an automatic laser analyser (Coulter LS 200, Coulter Corp., Miami, FL, USA) following the methodology described in van Reeuwijk (1992) and Siiro (2002): 5 cm^3 of sediment from each sample were pre-treated to remove organic matter, carbonates and iron oxides, prior to the laser analyses. Clay mineralogy was studied by X-ray diffractometry (XRD) at the Senckenberg Institute in Wilhelmshaven, Germany, using the procedure described in Räsänen *et al.* (1998). Smear slides of clay (diameter <2 μm) separates were pre-treated with Mg^{++}, K^{+} and ethylene glycol prior to analysis.

Palynological analyses were performed at the Catholic University of Goiás in Goiania, Brazil. From each sample, 8 cm^3 of sediment was pre-treated using an adaptation of the standard methodology used by Hoorn (1994c) and Ybert *et al.* (1992). The pre-treatment comprised: (i) manual mixing of the sediment; (ii) addition and mixing of the exotic pollen *Lycopodium clavatum* as an aid for concentration calculations; (iii) removal of carbonates, the inorganic silicate fraction and organic debris; and, (iv) the mounting of samples in glycerine. Sporomorphs were counted until a minimum pollen sum of *ca* 300 angiosperms and gymnosperms was achieved. From these data, palynological concentration and percentage diagrams were constructed.

All palynomorphs were compared with modern analogues to reconstruct the plant palaeo-communities. Based on this comparison and available literature (e.g. Caratini *et al.*, 1973, 1980; Lorente, 1986; Hoorn, 1994c; Plaziat, 1995; Yamamoto, 1995; Leite, 1997; Colinvaux *et al.*, 1999; Rull, 2001), the fossil taxa are grouped into five main assemblages according to their botanical affinities with modern depositional environments (see below).

SEDIMENTOLOGY OF THE NAUTA FORMATION

The Nauta Formation is characterized by laterally and vertically variable facies, dominated by patchy to locally pervasively bioturbated siliciclastic sediments, with some calcareous layers (Fig. 4). Abundant clay intraclasts and/or mud blocks are present within a sand matrix, producing a brecciated texture that is typical of this formation (Fig. 4D). The lithology varies between fine-grained muddy to silty yellow, red, brown to light grey or beige sand and grey mud. Coarse- to medium-grained sand, calcareous sands and light grey to beige marls are also locally observed. The mud comprises bluish smectitic to reddish kaolinitic clay with a subordinate component of illite

and near-surface aluminium-chlorite (Räsänen *et al.*, 1998). The latter reflects recent strong chemical weathering in a humid tropical climate. The clay mineralogy distinguishes the Nauta Formation from the underlying smectite-rich, Pebas Formation (see Räsänen *et al.*, 1998).

The Nauta facies are grouped into three main facies associations (FA1–FA3) based on physical sedimentary structures: mud-draped trough cross-stratified sand (FA1); inclined heterolithic (sand–mud) stratification (FA2); and, horizontally stratified sand–mud couplets (FA3). All facies associations are characterized by a cyclic deposition of metre- to decimetre-scale sand–mud couplets. The metre-scale cycles consist of *ca* 60–100 cm thick massive to parallel-laminated sand sets capped by *ca* 5–80 cm thick brecciated to rhythmically laminated mud; whereas the decimetre-scale cycles are comprised of *ca* 20–50 cm thick, locally pervasively bioturbated, ripple cross-stratified sand sets capped by slightly to non-bioturbated massive appearing mud sets. Each facies association is described in detail below. Their detailed ichnology and palynology are described separately. A summary of the facies associations is presented in Table 2.

Facies associations

FA1 – mud-draped trough cross-stratified sand (sections 1, 4 & 5)

FA1 is characterized by 0·4–0·5 m thick, trough-shaped sand beds (Fig. 4A and C) arranged mainly in up to 5 m thick upward-coarsening successions (e.g. section 1, Figs 6 and 7). The beds are trough cross-stratified. Locally, plane-parallel lamination, current-ripple lamination, rare wave and backflow ripples, and mud drapes are observed (Fig. 4C). Intercalated mud layers are *ca* 5–10 to 40 cm thick with individual drapes ranging from a few millimetres to several centimetres in thickness. Mud drapes are mainly preserved in the basal parts of the troughs, and are internally laminated, massive-appearing or brecciated. Moreover, rip-up mud clasts are observed along bedding planes, sometimes lateral to the mud drapes (Fig. 4H).

FA1 includes two sub-facies: (i) organic-poor, trough cross-strata (FA1A; base of section 1, with inclined master bedding to the north-east, and southern base of section 4, with inclined master bedding to the south–south-west; Figs 5 and 11); and (ii) organic-rich rhythmites (FA1B; base of section 5, Fig. 4A) preserved in the troughs, though locally arranged in upward-fining clinoforms, with inclined master bedding to the south-east and to the north-west (Fig. 16).

FA1B shows organic debris draping ripple foresets in trough cross-laminated sets, and locally climbing ripples (Fig. 4A and E). The rhythmites in FA1B are parallel-laminated (Fig. 4E) and consist of an alternation of millimetre-scale sand–mud couplets that may contain current ripples where the sand content increases. Locally, each of the millimetre-scale couplets may contain, in addition to one sand and one mud lamina, an organic-rich lamina and/or one lamina of elemental sulphur, making each cycle accordingly a triplet and/or a tetraplet (Fig. 4E). Pyrite nodules are observed along the organic-rich laminae (Fig. 4E).

FA1 shows a low degree of bioturbation (i.i. = 1–2), characterized by diminutive (<1 mm in diameter) trace fossils concentrated in the mud drapes of FA1A. In some cases, lamination is completely destroyed by these small traces, but where lamination is preserved, mud couplets and rhythmites are common in these beds. Bioturbation of sand locally occurs, and may be pervasive in FA1A, but only very local in FA1B.

Fossil pollen grains are found only in the rhythmically laminated organic-rich sediments of FA1B (see below). The rhythmites contain pervasive soft sediment deformation composed of contorted laminae (arranged in upward thickening, deformed vs. non-deformed, *ca* 7 cm thick cycles; see 1–1·4 m at log in Fig. 16C), convolute bedding, small-scale load casts with ball-and-flame structures, microfaulting, and slumping with translated and rotated blocks.

Palaeocurrent data measured from the troughs in FA1A show a bi-directional SW–NE orientation at section 1 (Figs 6 and 7; Table 2) and a unidirectional orientation towards the SW at section 4 (Fig. 12; Table 2), whereas in FA1B foresets indicate a consistent SW-oriented transport direction (Fig. 16B and C; Table 2) in section 5.

FA2 – inclined heterolithic sand–mud stratification (sections 2–5)

FA2 consists of up to 10 m thick upward-fining successions of high-angle (<30°) to low-angle (1–2°) inclined heterolithic stratification (IHS; Fig. 4B). The IHS successions are defined by 0·2–1 m thick sand to mud-dominated couplets with variable strength of bioturbation (i.i. = 1–4). The transition from sand to mud in the couplets is typically gradational. The sandy part of the couplets (*ca* 10–60 cm thick sets; locally 0·9–2·5 m thick cosets, see uppermost part of log in

Table 2. Summary of sub-facies associations and their main characteristics.

Sub-facies/ association	Characteristic physical sedimentary structures	Vertical trend of individual sets	Thickness/shape of individual sets	Main type of transport	Average orientation of palaeocurrents (P) in trend°/plunge° and major bounding surfaces (MBS) in declination°/inclination°	Degree of bioturbation and trace fossils
FA1A/Organic-poor mud draped trough cross-stratified sand	Trough cross-strata Concave to ripple laminae Backflow ripples Mud drapes	Slightly upward coarsening	m–cm/trough to lensoidal	Traction Saltation Suspension	Section 1 Opposite P: range from 340–45°/18–10° to 190–245°/20°; Orthogonal P: 85°/20°, 125°/20° ($n = 27$) Section 4 Mean P: 219°/19° ($n = 37$) MBS: 20°/5° ($n = 1$), 55°/5° ($n = 1$), 252°/7° ($n = 4$)	Low degree of bioturbation In sand: *Skolithos*, *Thalassinoides*, *Teichichnus*, *Taenidium*, *Planolites*, *Scolicia* (*Laminites*), *Ophiomorpha*, *Chondrites* In Mud: *Planolites*, *Palaeophycus*, *Thalassinoides*, *Rhizocorallium*, *Cylindrichnus*, *Gyrolithes*
FA1B/Organic-rich rhythmites in trough cross-strata	In couplets, triplets or tetraplets Climbing ripples Rip-up mud clasts Soft sediment deformation	Upward fining	mm/trough to lensoidal	Traction (sand, mud floccules) Suspension Fluidized flow	Section 5 Mean rhythmites P: 211°/12° Mean ripples P: 210°/15° Mean flat laminae P: 196°/12° ($n = 57$) ≈MBS: 233°/6° ($n = 3$), 148°/17° ($n = 3$)	In sand: *Thalassinoides*, *Arenicolites*, *Planolites*, *Psilonichnus*
FA2A/ Thoroughly bioturbated IHS	Inclined heterolithic strata Ripple laminae Wavy to undulatory bedding Tangential current ripples	Upward fining	cm–dm/tabular-lenticular-concave	Suspension Traction	Section 2 Main Ripples P: 15°/17°, 95°/7°, 290°/10° ($n = 5$) MBS: 216°/15° ($n = 15$) Section 3 P: 316°/10° to 155°/10° ($n = 6$) Section 4 Mean ripples P: 198°/23° ($n = 2$) MBS: 75°/5° ($n = 1$)	High degree of bioturbation *Planolites*, *Chondrites*, *Scolicia* (*Laminites*), *Thalassinoides*, *Skolithos*, *Taenidium*, *Psilonichnus*, *Rhizocorallium*, *Palaeophycus*, *Teichichnus*, *Asterosoma*, *Arenicolites*, root traces

Table 2. (Continued.)

Sub-facies/ association	Characteristic physical sedimentary structures	Vertical trend of individual sets	Thickness/shape of individual sets	Main type of transport	Average orientation of palaeocurrents (P) in trend°/plunge° and major bounding surfaces (MBS) in declination°/inclination°	Degree of bioturbation and trace fossils
FA2B/ Rhythmites within IHS	Tidal rhythmites In couplets, triplets Inclined heterolithic strata	Upward fining	cm–mm/tabular	Traction (sand, mud floccules) Suspension	Not measured	*Scolicia*, *Planolites*, *Skolithos*, *Thalassinoides*, *Rhizocorallium*, *Taenidium*, *Teichichnus*, *Psilonichnus*
FA2C/Brecciated IHS	Brecciated mud in sand/mud matrix – rip-up mud blocks/ clasts Inclined heterolithic strata	Upward fining	dm/irregular to wedge-shaped	Suspension Traction Saltation Rheological flow	Not measured	*Planolites*, *Thalassinoides*, *Teichichnus*, *Cylindrichnus*, *Gyrolithes*, *Palaeophycus*, *Arenicolites*, *Skolithos*, *Psilonichnus*, *Taenidium*
FA3A/ Horizontally stratified sand-mud couplets	Plane parallel strata Hummocky cross-strata Flaser bedding Backflow ripples Synaeresis cracks	Upward coarsening	cm–dm/wedge -tabular to trough Laterally continuous at outcrop scale	Traction Suspension	Not measured	Moderate degree of bioturbation *Taenidium*, *Thalassinoides*, *Planolites*, *Chondrites*, *Skolithos*, *Ophiomorpha*, *Rhizocorallium*
FA3B/ Horizontally stratified sand-marly mud couplets	Plane-parallel strata Flaser and lenticular bedding Double mud layering Organic-rich ripple laminae	Upward fining	cm–dm/tabular Laterally continuous at outcrop scale	Traction Suspension Precipitation	Section 1 P: 60°/20° & 180°/25° (n = 2) MBS: 20°/10° (n = 1)	In sand: *Skolithos*, *Thalassinoides*, *Teichichnus*, *Siphonites*, *Rhizocorallium*, *Arenicolites*, *Monocraterion* In mud: similar to FA1

P = palaeocurrents, MBS = major bounding surfaces.

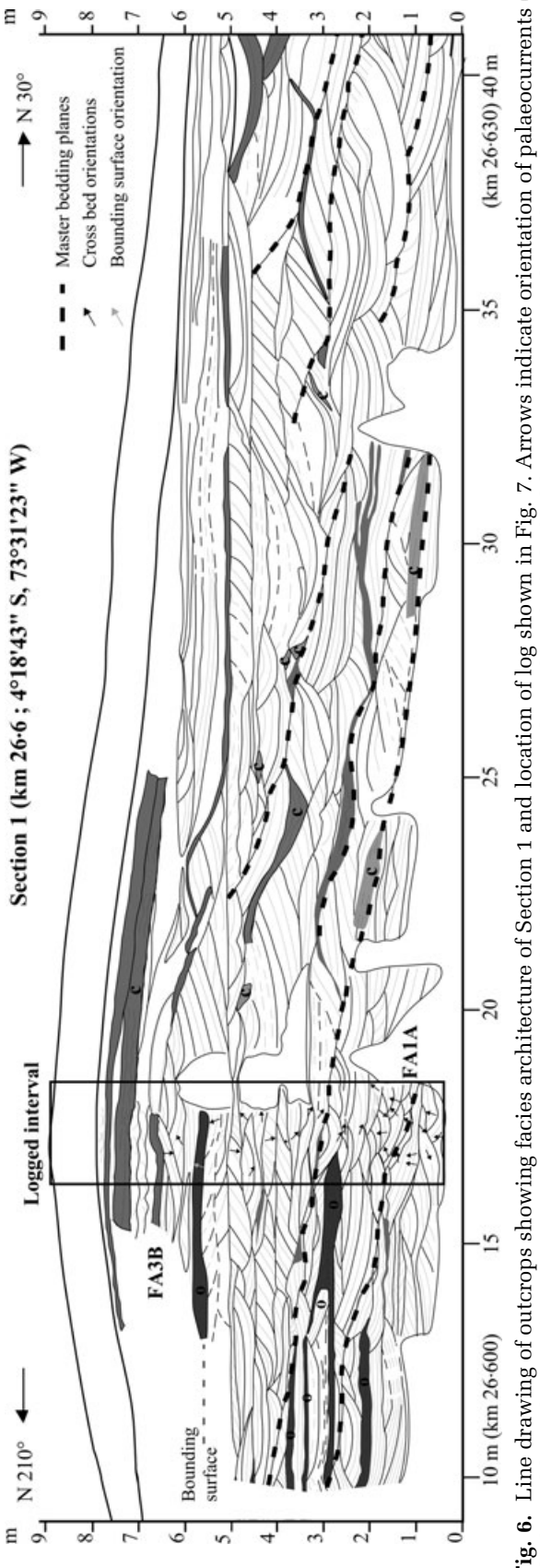

Fig. 6. Line drawing of outcrops showing facies architecture of Section 1 and location of log shown in Fig. 7. Arrows indicate orientation of palaeocurrents (in black) and bounding surface (in grey). Orientation of master bedding planes are indicated by thick dashed lines. See Fig. 5 for legend.

Fig. 16C) shows trough to tabular cross-stratification grading upwards to plane-parallel stratification and ripple lamination. This includes current and wave ripples, with organic debris occasionally draping the troughs and foresets of the ripples (e.g. Fig. 9). Sandy strata are amalgamated and lenticular, particularly near the top of FA2 units, and contain current-backflow ripples at their base (see Fig. 16A and C).

Like the mud layers in FA1, the mud-dominated component of the IHS couplets (generally *ca* 10–80 cm thick layers, but locally as thin as 2–5 cm and as thick as 0·9–2·4 m) is either massive, parallel-laminated or brecciated (e.g. see Fig. 4D). Internally, the muddy components fine upwards. The mud in the couplets includes a subordinate amount of sand arranged in flat lenticular- to wavy-bedded and tangential current-ripples. The mud-dominated components of the couplets commonly show irregular and undulatory lower contacts with the sand dominated part of the couplets. Oxidized and sand-filled shrinkage cracks (e.g. Fig. 11 at c. 0·2–0·25 m in the log) were observed in the FA2 mud.

FA2 is subdivided into three sub-facies: locally thoroughly bioturbated IHS (FA2A; base of section 3; Figs 10 and 11), rhythmically bedded IHS (FA2B; base of section 4; Figs 12–15) and brecciated IHS (FA2C; base of section 4; Figs 12–14). FA2A shows the highest degree of biological churning although mud laminae are locally preserved (locally i.i. = 2–4, Figs 13–15). FA2B, indicating moderate to low bioturbation (i.i. = 1–2), is characterized by parallel-laminated rhythmites (Fig. 4F) that occur in the mud-dominated parts of the sand–mud couplets. The rhythmites are arranged in *ca* 5 cm thick groups of 12–14 thin (individually up to 7 mm thick) laminae separated by *ca* 2 cm thick sandy layers (cf. Räsänen *et al.*, 1998, their fig. 4.9; Fig. 4F and log at 0–1·6 m in Fig. 14). Each of the 12–14 laminae is composed of a millimetre-scale sand–mud couplet. Finally, FA2C, with the lowest amount of bioturbation (i.i. typically = 1, locally 2), consists of sand–mud couplets comprising wedge-shaped sets that contain abundant irregular mud clasts/blocks set in a sand matrix (Figs 4D and 13).

Local palaeocurrent data measured from troughs within FA2 show a dominant NNW-oriented mode (Fig. 10; Table 2) with subordinate SE- and SW-oriented modes (Figs 10 and 12; Table 2), whereas the tabular cross-stratified sets show a subordinate NNE-oriented mode and the

bounding surfaces of the IHS deposits dip mainly towards the SW (Fig. 9; Table 2).

Locally, listric normal faults (e.g. Fig. 10: F1–F5) are observed affecting FA2. The faults show curved and bifurcating slip surfaces truncated by the stratification of the overlying facies association (FA3, see below). The general strike of the faults is WNW–ESE (average strike: N 287°), with an average dip of 35° southwards, and vertical offsets of *ca* 0·5 m. Moreover, bifurcating microfaults are present within rhythmites of FA2B.

FA3 – horizontally stratified sand–mud couplets (sections 1 & 3)

The horizontally stratified beds of FA3 are characterized by 0·6–0·8 m thick sand–mud couplets with a moderate degree of bioturbation (i.i. = 1–3; upper part of Figs 6, 7, 10 and 11). The beds are arranged in upward-fining successions. The sand contains trough- and tabular cross-stratification, plane-parallel to undulatory stratification changing upwards to lamination, current ripples dipping in opposite directions from set to set, wavy to bifurcating flaser bedding, and millimetre-scale, sand–mud rhythmites (upper part of log in Fig. 11). Mud sets are 10–30 cm thick and stratified to massive in appearance. Mud drapes both the stoss and lee sides of the ripples, and internally show a full range of flaser and lenticular bedding styles, plane parallel lamination, and rarely, organic-debris laminae. Rip-up mud clasts are also observed.

FA3 is divided into two sub-facies: a siliciclastic unit (FA3A; top of section 3) and a calcareous unit (FA3B; top of section 1). FA3A is characterized by massive-appearing, *ca* 0·7–1·8 m thick, sandy cosets with brecciated clay clasts at the base (see log at *ca* 2·7–3·2 m and at *ca* 6 m in Fig. 11), and abundant sand–mud rhythmites in the mud-dominated parts of the sand–mud couplets, especially towards the top (see log at 9·2–9·6 m in Fig. 11) of this sub-facies. FA3B consists of sand–marly mud couplets with trough-shaped layers including limestone nodules; these layers laterally correspond to the muddy part of the couplets (Figs 6 and 7). Each calcareous couplet consists of stratified, trough cross-laminated to parallel-laminated sand capped by parallel-laminated mud, organic-rich, ripple-laminated muddy sand (Fig. 7), calcareous mud, marl, or millimetre-scale rhythmites. Rhythmites in FA3B are of millimetre scale and comprise sand interlaminated with fissile calcareous sandy mud with sand lenses, organic-debris laminae, and double mud drapes (Fig. 7). The double mud drapes separate a thin sand lamina from a thicker one. Some rhythmites are triplets consisting of interlaminated calcareous sand, sandy silt and weakly laminated marls that are usually laterally equivalent to the organic-rich muddy sand layers. Sand-filled shrinkage cracks were observed in the FA3B mud.

Bioturbation in FA3A is locally pervasive in the rhythmically laminated parts (see log at 8–10 m in Fig. 11 where i.i. is up to 3). Traces are mostly vertically oriented and decrease in size upwards. Trace fossils in FA3B are concentrated in the uppermost metre within sand (i.i. = 1–2) and have an above-average size (*ca* 1 cm in diameter) and low diversity. The traces are present at the base of lower angle cross-laminated toe sets.

Palaeocurrent measurements taken from cross-stratified sets in FA3B show a bimodal orientation towards the NE and south, with a major bounding surface dipping towards the NNE (Fig. 7; Table 2).

Trace fossil assemblages

The degree of bioturbation in each of the three facies associations ranges from low in the trough cross-bedded facies (FA1), through moderate in the horizontally bedded facies (FA3), to locally high in the IHS facies (FA2); the style of bioturbation is described below and summarized in Table 2 (see also Fig. 17).

FA1 – ichnology

Except for some sand bedsets, where bioturbation is locally pervasive, ichnofossils in FA1 are mostly restricted to the mud drapes preserved in the troughs. The bioturbated sands of the organic-poor trough cross-bedded facies (FA1A; observed in the southern end of section 4) are dominated by *Skolithos* (abundant to rare), cross-cutting *Thalassinoides* (abundant), and *Teichichnus* (rare to moderate). Locally, *Taenidium*, subtle *Planolites*, *Scolicia* variants (rare; typically *Laminites*), *Ophiomorpha* (rare) and *Chondrites* (rare) are present. *Planolites* and *Chondrites* cross-cut *Teichichnus* and *Thalassinoides*. Bioturbation within the organic-rich trough cross-bedded facies (FA1B) is constrained within one semi-continuous sandy horizon that contains *Thalassinoides*, *Arenicolites*, *Planolites* and *Psilonichnus*.

The ichnofossil assemblage in the mud units of FA1A consists of a sporadically distributed, though locally highly abundant (i.i. = 2), suite of diminutive (<1 mm diameter) *Planolites* and *Palaeophycus*, large *Rhizocorallium*, and rare

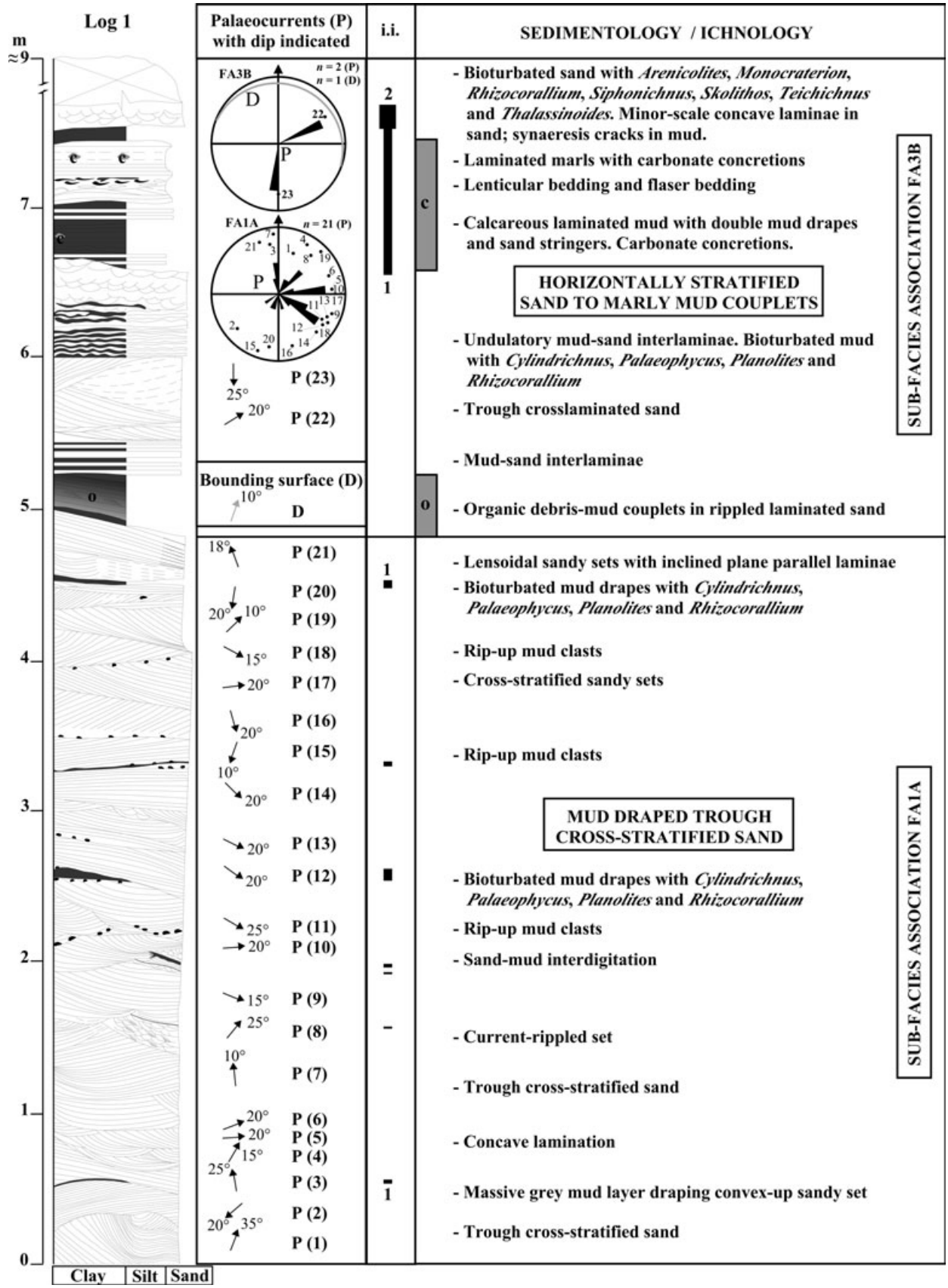
Log 1
m
≈9
7
6
5
4
3
2
1
0
Clay
Silt
Sand
Palaeocurrents (P) with dip indicated
i.i.
SEDIMENTOLOGY / ICHNOLOGY
FA3B
n = 2 (P)
n = 1 (D)
D
P
22
23
FA1A
n = 21 (P)
P (23)
25°
20°
P (22)
Bounding surface (D)
10°
D
- Bioturbated sand with Arenicolites, Monocraterion, Rhizocorallium, Siphonichnus, Skolithos, Teichichnus and Thalassinoides. Minor-scale concave laminae in sand; synaeresis cracks in mud.
- Laminated marls with carbonate concretions
- Lenticular bedding and flaser bedding
- Calcareous laminated mud with double mud drapes and sand stringers. Carbonate concretions.
HORIZONTALLY STRATIFIED SAND TO MARLY MUD COUPLETS
- Undulatory mud-sand interlaminae. Bioturbated mud with Cylindrichnus, Palaeophycus, Planolites and Rhizocorallium
- Trough crosslaminated sand
- Mud-sand interlaminae
- Organic debris-mud couplets in rippled laminated sand
SUB-FACIES ASSOCIATION FA3B
P (21)
P (20)
P (19)
P (18)
P (17)
P (16)
P (15)
P (14)
P (13)
P (12)
P (11)
P (10)
P (9)
P (8)
P (7)
P (6)
P (5)
P (4)
P (3)
P (2)
P (1)
- Lensoidal sandy sets with inclined plane parallel laminae
- Bioturbated mud drapes with Cylindrichnus, Palaeophycus, Planolites and Rhizocorallium
- Rip-up mud clasts
- Cross-stratified sandy sets
- Rip-up mud clasts
MUD DRAPED TROUGH CROSS-STRATIFIED SAND
- Bioturbated mud drapes with Cylindrichnus, Palaeophycus, Planolites and Rhizocorallium
- Rip-up mud clasts
- Sand-mud interdigitation
- Current-rippled set
- Trough cross-stratified sand
- Concave lamination
- Massive grey mud layer draping convex-up sandy set
- Trough cross-stratified sand
SUB-FACIES ASSOCIATION FA1A

Cylindrichnus and *Gyrolithes*. Only one to two of the aforementioned trace fossils, most commonly *Planolites* and *Palaeophycus* dominate the burrowed zones.

FA2 – ichnology

The IHS facies (FA2) is characterized by locally thoroughly bioturbated units with mud-filled burrows descending from the mud beds into the sand (e.g. Fig. 17G). Despite the high degree of biogenic overturn (i.i. up to 4), the ichnoassemblages comprise a low diversity of traces. The mud dominantly contains a low-diversity *Planolites–Chondrites* association, in which the traces decrease in size and become indistinct upwards, and shows lower diversity towards the top of the IHS successions. In contrast, the sand variably contains *Skolithos–Planolites* or *Laminites–Thalassinoides* ichnofossil associations. The *Skolithos–Planolites* association comprises rare to moderate *Skolithos* (diminutive to large and deep penetrating), and abundant large and small *Planolites*. The primary elements of the *Laminites–Thalassinoides* association are small to large, deep-penetrating *Laminites* (30 cm long, rare to moderate), and large (*ca* 2 cm in diameter) to medium (*ca* 1 cm in diameter) vertically oriented *Thalassinoides* (abundant).

The three aforementioned trace fossil associations are locally accompanied by large *Taenidium*, large *Psilonichnus* (Fig. 17G), small *Rhizocorallium* (very rare), sporadically distributed *Palaeophycus* and well developed *Teichichnus*. Clusters of *Chondrites* are seen to reburrow *Thalassinoides*, whereas *Palaeophycus* or *Planolites* may reburrow *Psilonichnus* (Fig. 17G). Well-developed, mud-filled, unlined *Thalassinoides* descend into mud beds locally generating a *Glossifungites* assemblage.

Ichnoassemblages in the locally thoroughly bioturbated IHS facies (FA2A; i.i. = 1–4, locally 3–4; see section 4; Figs 12–15) are dominated by *Scolicia* (variant *Laminites*; *ca* 2 cm in diameter, Fig. 17A–C) or small (*ca* 3 mm in diameter) *Skolithos* and/or *Taenidium* fabrics. *Scolicia* is small to large; common to rare and deep penetrating. *Skolithos* is small to large, common to moderate, though becomes rare upwards, sand-filled and deep-penetrating. *Taenidium* is medium-sized, common and penetrates to medium depths. Associated traces are large *Planolites* (common) to small *Planolites* (locally pervasive), medium-sized *Thalassinoides* (moderate, sand-filled, deep-penetrating), small *Rhizocorallium* (rare), diminutive *Chondrites* (common to sporadically distributed), and large *Palaeophycus* (rare) to small *Palaeophycus* (common, sporadically distributed, descends from sand). Towards the top of the IHS units, where mud-dominated (see Figs 14 and 15), *Skolithos*, *Planolites* and *Palaeophycus* dominate the assemblages, traces are smaller (average 3 mm in diameter), burrowing is pervasive (i.i. = 3–4) but lamination is locally preserved. Further upwards, *Taenidium*-dominated assemblages with *Planolites*, *Palaeophycus*, robust *Chondrites* and rare *Skolithos* are observed. This gives way to a *Palaeophycus–Planolites–Chondrites* dominated assemblage and ultimately to a *Palaeophycus–Planolites* ichnofabric. Additionally, clusters of *Arenicolites* (rare), and palaeoroot traces (rare) occur.

Bioturbation within the rhythmically laminated inclined heterolithic facies (FA2B; i.i. = 1–2) also includes *Laminites* (average 7–10 mm in diameter; common), *Planolites* (3–5 mm in diameter; common-to-abundant), sand-filled *Skolithos* (moderate), *Thalassinoides*, *Rhizocorallium*, sand-filled *Taenidium* (see Fig. 17D), small-to-large *Teichichnus* (13 cm long) in locally deformed sand laminae, and *Psilonichnus*. *Laminites* and *Planolites* are commonly observed together, typically meandering along bedding planes. Moreover, *Laminites* takes on a *Taenidium* appearance in the finer-grained rhythmites (Fig. 17D). Finally, *Thalassinoides* and *Teichichnus* form an association in the transition from sand-dominated to mud-dominated rhythmites.

Bioturbation in the brecciated inclined heterolithic facies (FA2C; i.i. = 1–2) includes an association of small to diminutive ichnofossils, including (see Fig. 13) *Planolites* (common) and *Thalassinoides*, rare *Teichichnus* (2–7 cm long; observed crossing a sand/clay clast boundary), rare *Cylindrichnus*, *Gyrolithes* or compacted ?*Skolithos*, *Palaeophycus* (common), rare *Arenicolites*, rare *Skolithos* (*ca* 3 mm in diameter), large

Fig. 7. Graphic log of section 1. Rose diagrams of palaeocurrents with scattered dots for illustration of cross-bed dip (separately for FA1A and FA3B); great circle represents the orientation of bounding surface (see Fig. 6). The scattered dots are numbered consecutively according to location of measurement in log from bottom to top. Note wide variability between consecutive measurements. See Fig. 6 for location and Fig. 5 for key to legend and ichnofabric index (i.i.).

Psilonichnus (*ca* 4 cm in diameter; inclined tubular shaped) and *Taenidium*. *Skolithos*, *Planolites* and *Thalassinoides* cross-cut *Psilonichnus*.

FA3 – ichnology

In sub-facies FA3A, bioturbation primarily comprises vertically oriented trace fossils (uppermost part of log in Figs 11 and 17E). The trace fossils show a decrease in size upwards (from *ca* 2 cm to <1 mm in diameter). Two assemblages were documented. The first is a *Taenidium*-associated assemblage including *Thalassinoides*, *Planolites* and well-developed *Taenidium* reburrowed by *Chondrites*/*Planolites*-like ichnofossils (i.i. = 1–2, Fig. 17F). The well-developed *Taenidium* cross-cuts rhythmically laminated sediment. The second assemblage is *Skolithos*-dominated and characterized by large *Skolithos*, *Taenidium*, *Ophiomorpha*, *Thalassinoides* (e.g. Fig. 17E, i.i. = 3; average *ca* 8 cm in diameter), *Planolites*, and exceptionally large unlined, inclined and passively filled trace fossils assigned to *Psilonichnus*. Diminutive (<1 mm in diameter), rare, sand-filled *Rhizocorallium* and *Skolithos* are dominant near the top of the succession.

Trace fossils associated with FA3B were observed in only one sandy horizon, which was homogenized by burrowing activity (i.i. = 2). The trace fossils are normally 7–8 mm in diameter. Two recurrent ichnofossil assemblages are present: (i) a *Skolithos*, sand-filled *Thalassinoides* and *Teichichnus* association; and (ii) a *Siphonichnus*–?*Rhizocorallium jenense*–*Arenicolites*–?*Monocraterion* association. Notably, *Thalassinoides* and *Siphonichnus* cross-cut *Teichichnus* and must represent the deepest ichnological tiers. Bioturbation within the mud is characterized by diminutive traces similar to the *Planolites*–*Palaeophycus*–*Thalassinoides* association described for the mud in FA1A (see above).

Palynology

Several samples from the organic-rich rhythmites (FA1B) at section 5 were palynologically studied. However, only one sample at *ca* 9 m depth (sample Na-99-104; see Fig. 16A for location) contained fossil pollen. The sample is characterized by a high diversity of pollen grains though in very low concentrations (47 species of palynomorphs were found from 337 pollen grains and four spore grains; Table 4). An exception is *Psilatricolporites varius*, which commonly shows a high concentration and represents 25·5% of the total palynomorph count (Table 4). Although the pollen grains of some dominant species are preserved as aggregated masses (e.g. in the case of *Psilatricolporites varius*, *Retitricolpites simplex* and *Retitricolporites milnei*), there is no evidence of reworking, even in grains with fine exine (e.g. *Psilatricolporites maculosus*), or those with high relief ornamentation such as the clavated *Crototricolpites* sp. or the echinated *Echiperiporites stelae*, which show complete preservation of their external surface. Moreover, there is no evidence of darker coloration which would indicate reworking and redeposition of the pollen grains. This suggests that the pollen grains came from a local source and underwent very little transport prior to deposition.

The palynomorphs can be grouped into five (1–5) assemblages (see methods and Table 4). Assemblages 1 and 2 share mangrove-related elements and represent 33·7% of the total pollen sum. Assemblage 1 (15·5%) includes *Psilatricolporites maculosus*, *Retitricolpites simplex*, *Retitricolporites* sp. and *Zonocostites* sp., and has the highest correlation with mangrove environments (cf. Rull, 2001; Table 4). Assemblage 2 (18·2%) is related to herbaceous back-mangrove swamp environments and includes species that develop under low salinity to fresh water conditions (e.g. *Cyperaceapollis*, *Monoporites annulatus*, *Psilatricolporites operculatus* and *P. triangularis*; Table 4). Assemblage 3 (14·4%) includes taxa related to rainforest or floodplain environments; dominant species are *Crototricolpites* sp., *Heterocolpites incomptus* and *Myrtaceidites* sp. (Table 4). Assemblage 4 (2·9%) comprises *Equimorphomonocolpites solitarius*, *Mauritiidites* sp., *Psilamonocolpites* sp. and *Retimonocolpites maximus*, which are related to palm swamp environments (Table 4). Assemblage 5, including species with unknown botanical affinity and with unknown or a wide range of environmental conditions, amounts to 49·0% of the identified palynomorphs (Table 4).

The Nauta pollen species association contains taxa of the late Early to early Middle Miocene *Psiladiporites*/*Crototricolpites* Concurrent Range Zone of Hoorn (1994b,c). A link with this palynological zone is also consistent with the occurrence of *Psiladiporites redundantes*, *Psilaperiporites minimus* and *Retitricolporites leticianus*, and by the absence of *Crassoretitriletes vanraadshoovenii*. However, the lack of biostratigraphic marker species in this zone and the stratigraphic position of the Nauta Formation, conformable above Late Miocene deposits of the Pebas Formation (Hoorn, 1994b,c; Räsänen *et al.*,

1998; Rebata-H. *et al.*, 2006), suggest the Nauta Formation is Late Miocene in age.

Palaeocurrent and bounding surface orientations

Compound rose diagrams of the palaeocurrent and bounding surface orientations are presented in Fig. 18. The planes have been plotted as lines (azimuth, dip) for illustration. The diagrams are based on the measurements presented separately for sections 1 to 5 in this paper (see above) and additional measurements in between the illustrated sections. The palaeocurrent data were measured from the dune troughs and cross-stratified sets. The compound diagram for palaeocurrent indicates a dominant SW-oriented mode (vector mean = 204°, mean cross-bed dip = 17°, $n = 384$; Fig. 18). At individual sections, the bounding surface orientations are at different angles, sometimes perpendicular or opposed, but mostly concordant to the palaeocurrents. The latter case denotes the difficulty of measuring the depositional planes with low inclination angles in near-strike cross-sections. The regional orientation of the bounding surfaces obtained in the compound rose diagram also indicates a dominant direction to the south-west (vector mean = 235°, mean dip = 13°, $n = 181$; Fig. 18), mainly reflecting the comparatively higher number of measurements at section 5.

Relationship within and between the different facies associations

As a result of the scattered nature of the outcrops in the study area, the three facies associations (FA1–3) were rarely seen together at one locality (see Fig. 19). Outcrops with one or two of the associations are widespread along the last *ca* 40 km of the Iquitos–Nauta Road. Two representative sections of the trough-crossbedded sands (FA1), sections 1 (FA1A) and 5 (FA1B), are oriented almost perpendicular to each other, and present near dip and strike views relative to the regional depositional dip to the south-west (see Figs 3, 6 and 16). From north to south, a grain-size gradient is seen along the road, with the sandier FA1A deposits, exposed more commonly north of km 18 (sand/mud ratio up to 6·7 in section 1), and muddier FA1B deposits exposed at km 3·5 (sand/mud ratio up to 1·8 in section 5). A third section of FA1, section 4 (Fig. 12), is almost parallel to section 1 and has an intermediate sand/mud ratio (up to 2·3). Organic debris is more dispersed within the muddier sections (e.g. in section 5, where the organic matter content reaches *ca* 70% in the rhythmites of FA1B), while its distribution is more restricted (concentrated within mud-dominated sets along the troughs) in the sandier sections (e.g. in section 1). Similar organic-rich triplet and tetraplet rhythmites to those present in section 5 are exposed along the Itaya River (see Fig. 3A for location). Deposits of FA1 are generally scoured by the IHS deposits of FA2 (e.g. Fig. 12 depicts FA2 truncating FA1). The base of the IHS deposits is generally an erosional, concave-upwards surface.

Inclined heterolithic stratified deposits (FA2), arranged in decimetre to metre-scale sand–mud couplets, are the most common facies association along the Iquitos–Nauta Road. Representative sections are exposed in sections 2–4; orientation of their bedding surfaces suggests that sections 2 and 4 are near-dip views, whereas section 3 is a near-strike view, again relative to the regional depositional dip (Figs 8–15). From the three subfacies described, the one that contains brecciated mud clasts/blocks in the muddy parts of the couplets (FA2C) is the most abundant; completely reworked mud beds are exposed along the road from km 6·7 till km 15. An individual FA2 succession typically shows FA2C passing vertically into FA2B and capped by FA2A (Fig. 13). The muddy deposits capping each succession (FA2A; see e.g. Figs 14 and 15) have restricted ichnofacies, but are most restricted towards the top (see e.g. log in Fig. 13). IHS successions composed of several cycles of FA2A (see Figs 8 and 9) are observed also with inclined, concave-up erosional surfaces separating individual cycles (e.g. surface X–X′ in Fig. 12). The rhythmically laminated layers (FA2B) within the mud-dominated parts of the couplets in the IHS deposits are only locally exposed.

Representative outcrops of the horizontally stratified FA3 are exposed in sections 1 and 3 (Figs 6 and 10). Commonly, FA3 caps the other two facies associations. The FA1–FA3 contact is conformable and locally marked by mud-drapes (Figs 6 and 7), whereas the FA2–FA3 contact is erosional, locally forming a concave-up surface marked by brecciated clay and onlapping cross-stratified sand (see Figs 10 and 11).

Because the regional depositional dip for the Nauta Formation is low, the 30 m elevation differences along the road can be used to construct a tentative vertical section through the formation (Fig. 19). At least three repetitive vertical cycles may be present in the formation; each

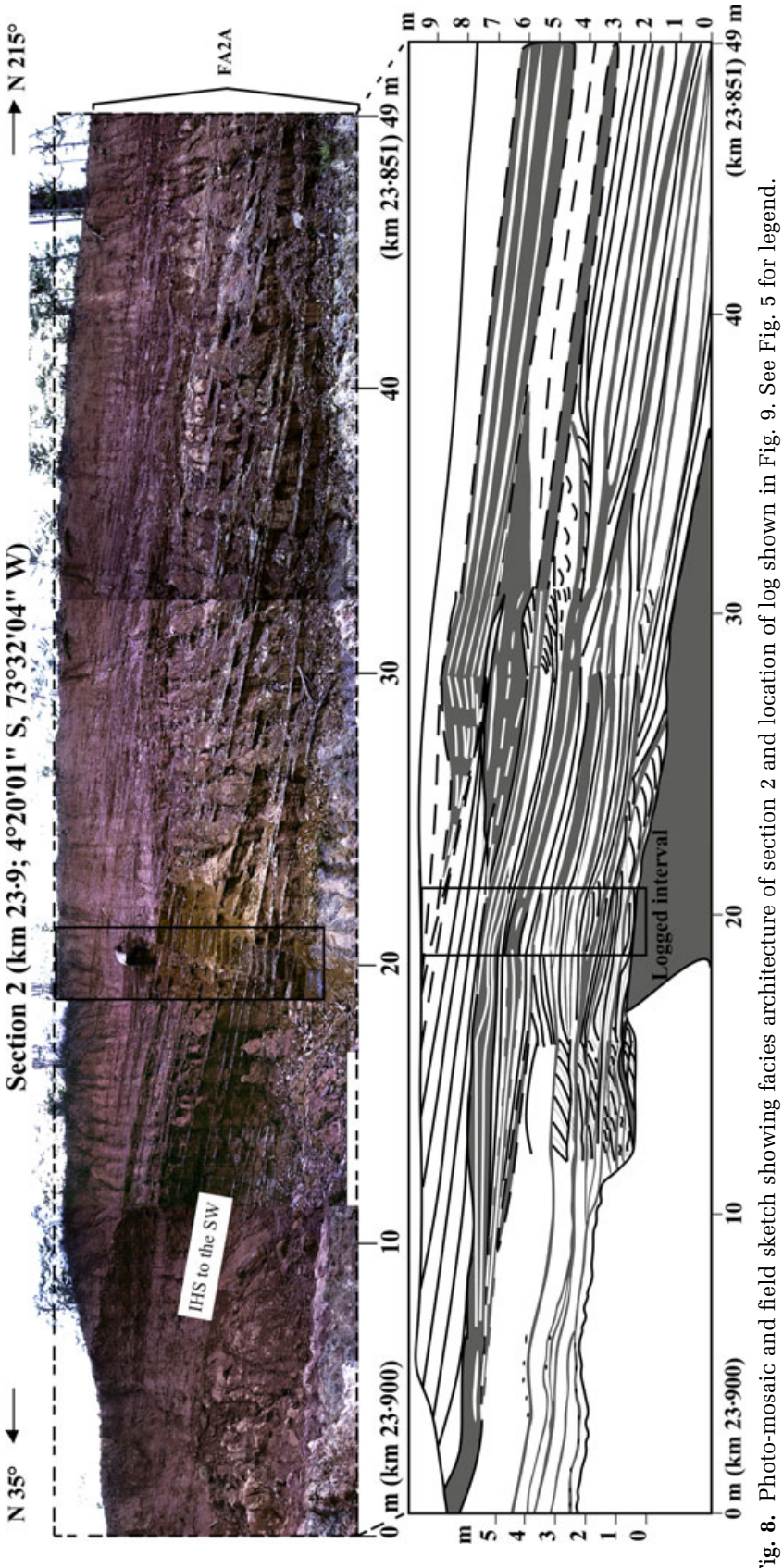

Fig. 8. Photo-mosaic and field sketch showing facies architecture of section 2 and location of log shown in Fig. 9. See Fig. 5 for legend.

ca 10–12 m thick and composed of a FA1–FA2–FA3 succession, where completely exposed.

INTERPRETATION

Depositional setting

The abundant, concave-up bounding surfaces within the Nauta Formation indicate a channelized setting (Fig. 19). The trough cross-stratified deposits of FA1 represent the migration of 3D compound dunes along the channel thalweg(s) and over bars. Back-flow ripples on the dunes are attributed to local counter-current flows. The inclined master bedding directions observed in the trough cross-bedded facies indicate the dominant bar migration direction. Similar facies architectures to the one presented as FA1, though at different scales, have been reported from compound dunes in subtidal to intertidal settings (e.g. Allen, 1980; Dalrymple, 1984; Le Bot & Trentesaux, 2004). However, because of the lack of evidence for sub-aerial exposure, it is probable that the Nauta dunes were deposited in a subtidal environment. Although the current velocity was generally high enough to inhibit mud accumulation, more discontinuous and less energetic currents locally allowed the preservation of mud drapes or millimetre-scale rhythmites in the dunes troughs and foresets. Mud particles apparently were deposited, by suspension settling and/or fallout during one or several slack-water periods, as laminated or massive mud. Most mud layers, when partially dewatered, were subsequently reworked by periodically strong currents and redeposited as brecciated clasts or blocks in a sand matrix; some of these mud blocks slid down inclined surfaces.

The IHS deposits of FA2 represent laterally accreting bars (in the sense of Thomas *et al.*, 1987). This interpretation is further supported by the perpendicular relationship between the depositional dip of the IHS deposits and the orientation of internal cross-stratified sets. IHS has most commonly been documented from tidally influenced point bars (cf. Thomas *et al.*, 1987); however, recently it has also been reported from straight, within-channel elongate (tidal) bars (cf. Dalrymple *et al.*, 2003). In the study area, the predominance of cross-sections with high-angle IHS, exposed in sections orientated parallel to the dominant palaeocurrent (Fig. 18), suggests the Nauta complex was composed of meandering rather than straight channels. Thus, FA2 most probably represents point bar deposits.

The horizontally stratified sand–mud couplets of FA3 are interpreted as shallow subtidal to intertidal flat deposits. The locally concave-up, mud-brecciated lower boundary of FA3A marks the scoured base of a channel, whereas the calcareous sediments (FA3B) probably resulted from sub-aqueous precipitation and vertical settling in shallow or abandoned channels. Furthermore, marly sets could have developed at times of stronger temperature stratification and their rhythmic sedimentation patterns (upper part of log in Fig. 7) may be related to changes in surface water productivity (Thunell *et al.*, 1991). This would have favoured the local precipitation of carbonates on the tidal flats.

The oxidized shrinkage cracks observed within mud in the lowest angle (1–2°) IHS beds are interpreted as incipient desiccation cracks. Their relationship with discrete palaeoroot penetration structures supports a sub-aerial exposure. However, the position of the desiccation cracks, immediately overlying sandy layers with a trace fossil assemblage indicative of normal marine conditions (see interpretation of trace fossil assemblages below), suggests that the emergence was ephemeral. In contrast, the sand-filled shrinkage cracks within FA2 and FA3B mud are interpreted as synaeresis cracks (sub-aqueous shrinkage cracks formed by the contraction of clay-rich sediments when submerged in a saline medium; cf. Plummer & Gostin, 1981). The interpretation of synaeresis processes causing sub-aqueous shrinkage cracks in natural conditions is currently debated. Layer-parallel contraction caused by compaction and burial, or seismic shocks have been suggested as most likely to cause interstratal dewatering and cracking of mud (e.g. Pratt, 1998; Tanner, 1998). Trace fossil evidence in FA3B (*Thalassinoides* and *Arenicolites* traces in the same bed as the synaeresis cracks) supports saline water conditions during crack formation.

An ideal vertical sequence, relating the three main facies associations observed, is FA1–FA2–FA3 (i.e. trough cross-stratified sands overtaken by inclined heterolithic strata and capped by horizontally bedded heteroliths; Fig. 19). This vertical sequence could reflect lateral migration of channels in the Nauta complex: dunes flooring the channels are overlain by point bars, which in turn, were overlain by tidal flat successions. A similar facies sequence in a channel complex has been described from the Lower Cretaceous

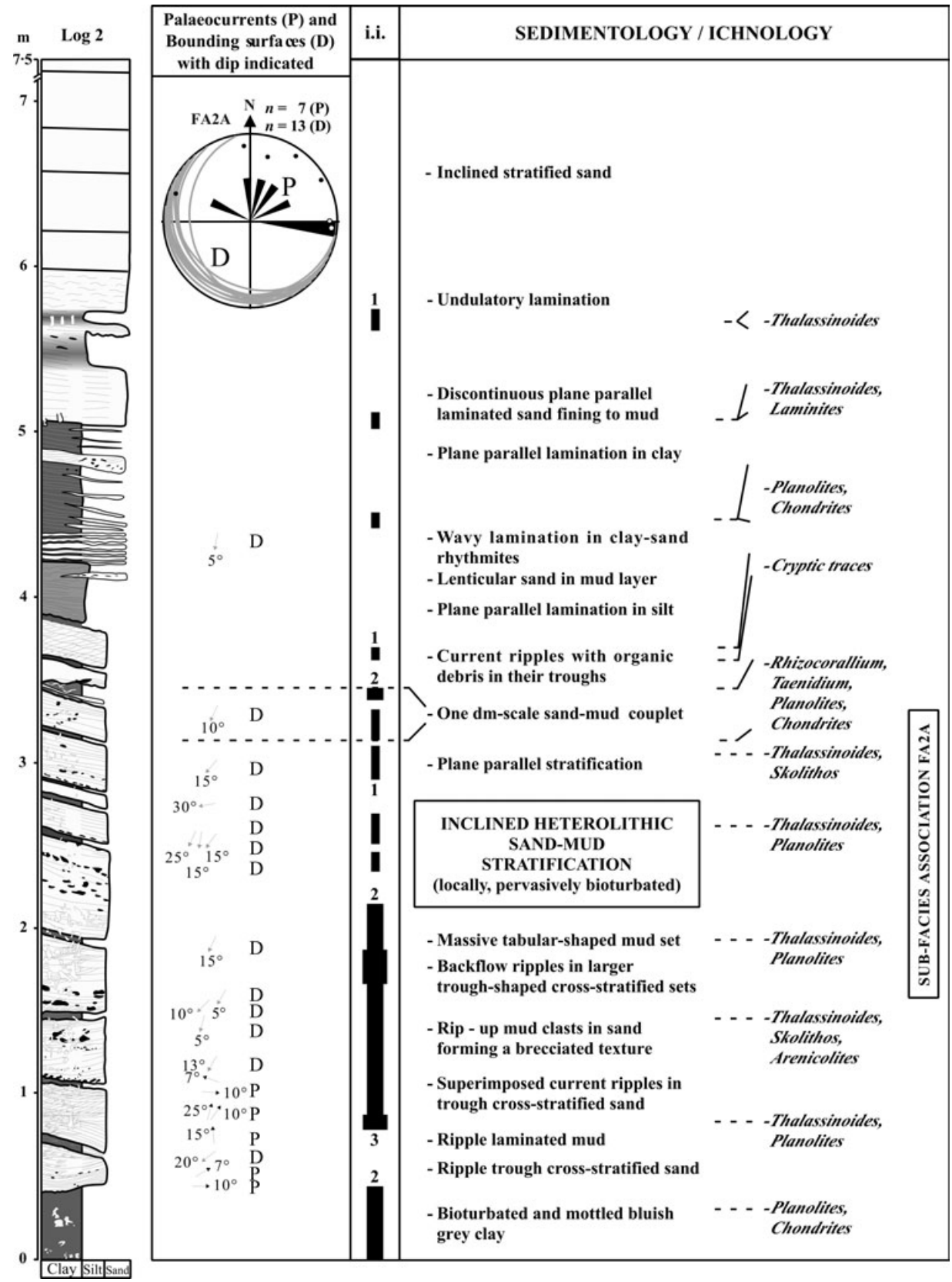

Fig. 9. Graphic log of section 2. Rose diagram of palaeocurrents with scattered dots for illustration of cross-bed dip (for FA2A); great circles are IHS bounding surfaces. See Fig. 8 for location and Fig. 5 for key to legend and ichnofabric index (i.i.).

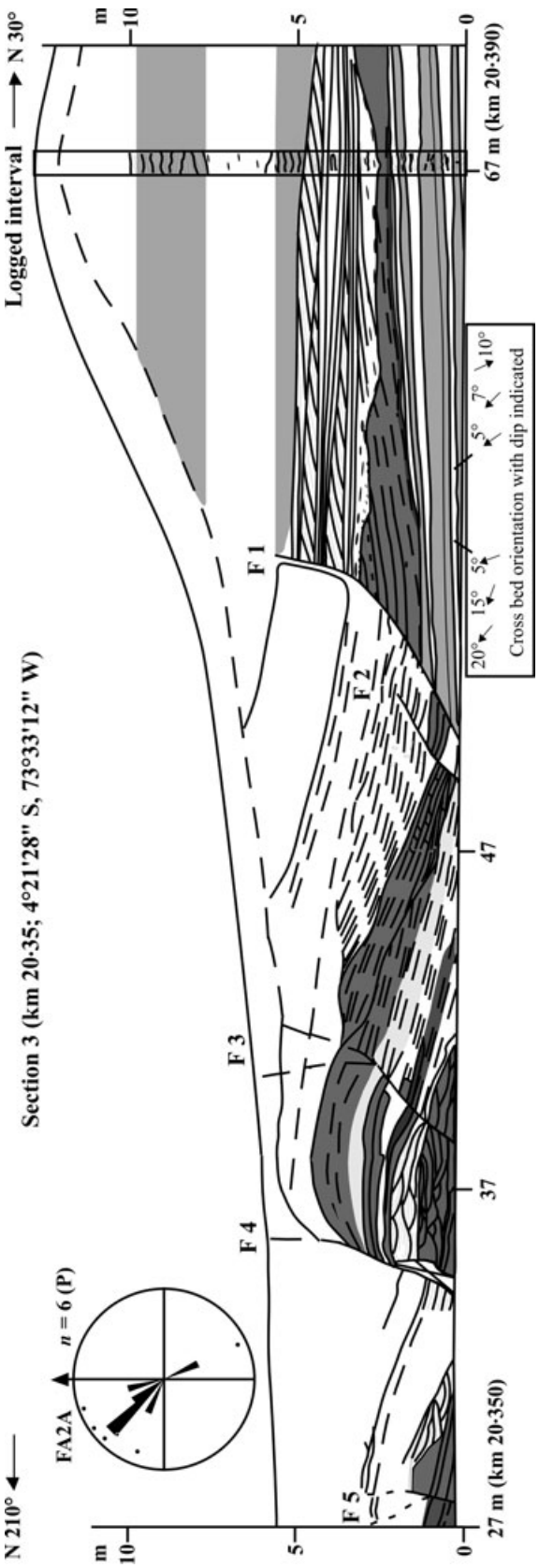

Fig. 10. Line drawing of outcrops showing facies architecture of section 3 and location of log shown in Fig. 11. Note listric faults (F1–F5). Rose diagram of palaeocurrents with scattered dots for illustration of cross-bed dip (for FA2A). See Fig. 5 for legend.

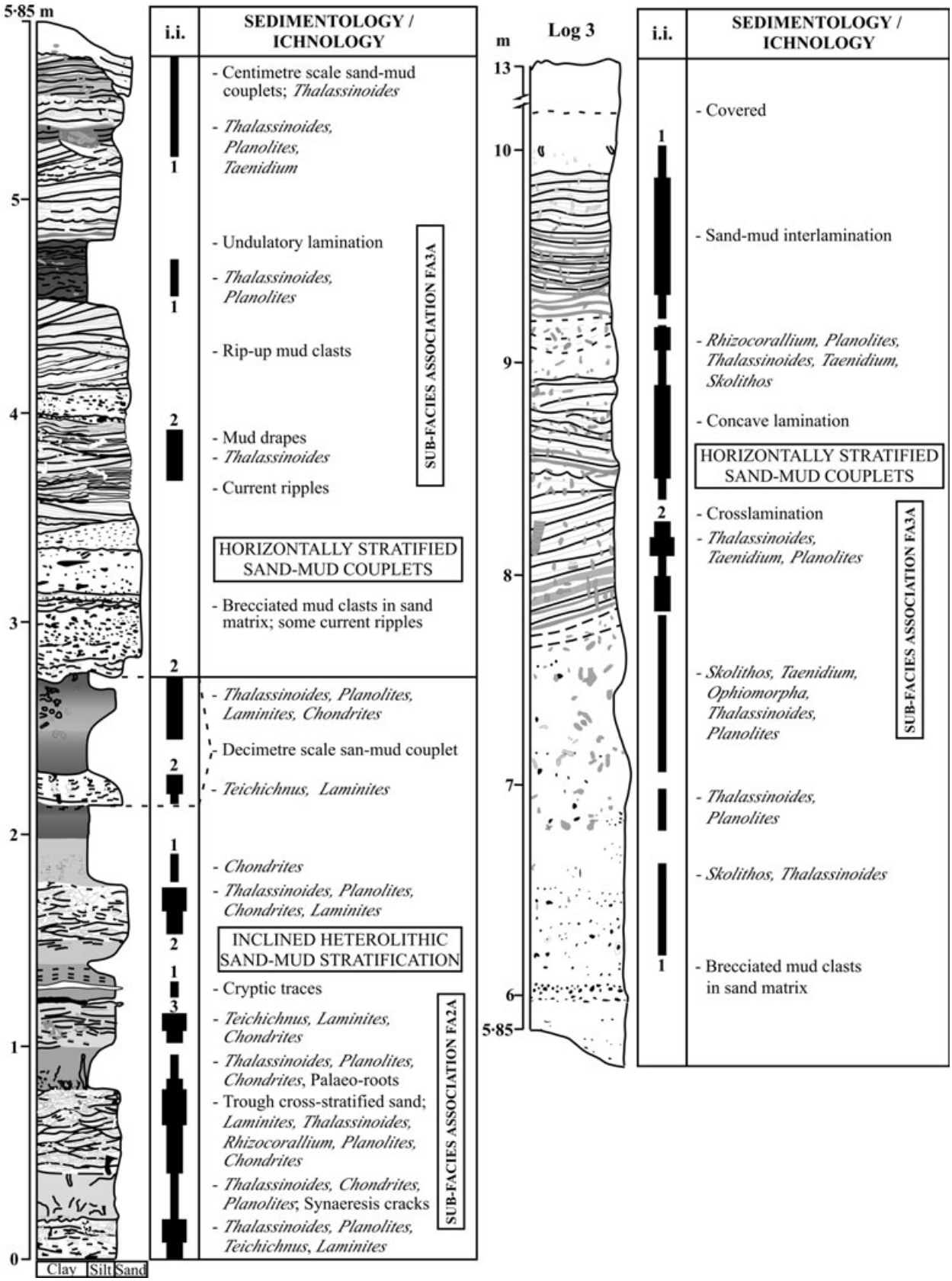

Fig. 11. Graphic log of Section 3. See Fig. 10 for location and Fig. 5 for key to legend and ichnofabric index (i.i).

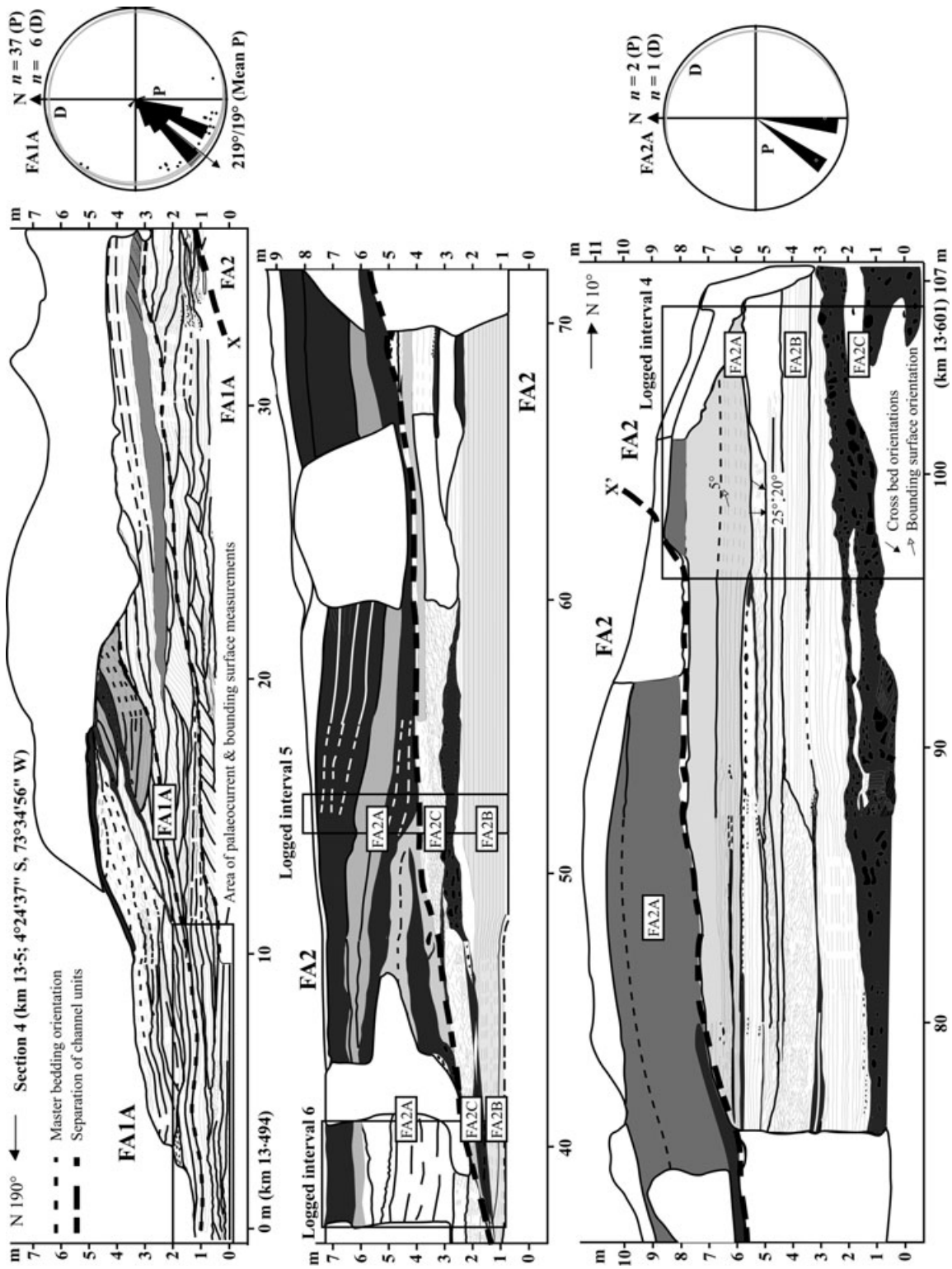

Fig. 12. Line drawing of outcrops showing facies architecture of section 4. Note location of the three logged intervals (numbered from 4 to 6) shown in Figs 13–15. Rose diagram of palaeocurrents with scattered dots for illustration of cross-bed dip (separately for FA1A and FA2A); great circles represent the orientation of major bounding surfaces. Location of measurements for FA1A indicated by rectangle in the southern end of outcrop. See Fig. 5 for legend.

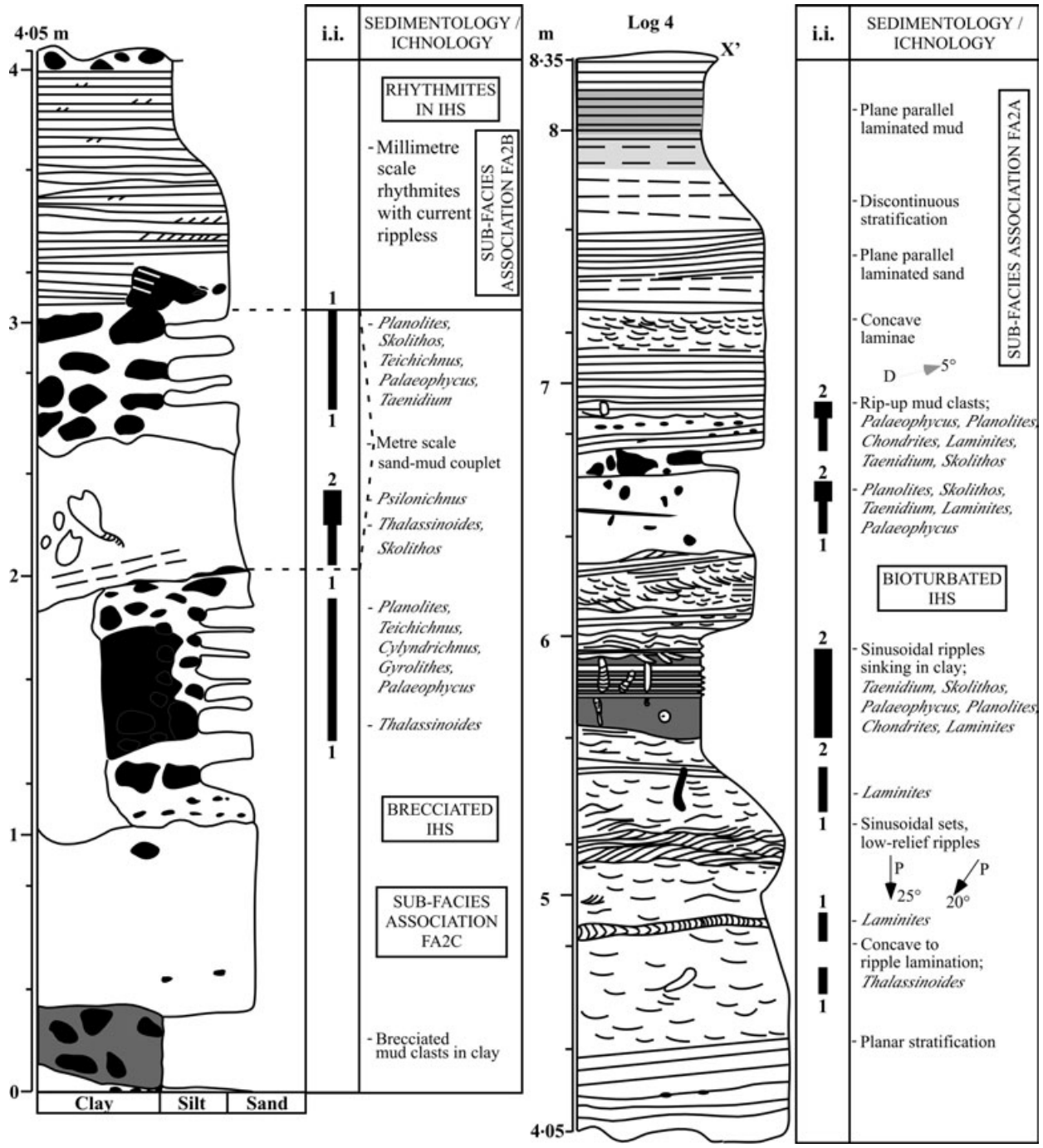

Fig. 13. Graphic log for interval 4 of Section 4. See Fig. 12 for location and Fig. 5 for key to legend and ichnofabric index (i.i.).

McMurray Formation (Pemberton *et al.*, 1982). The McMurray example is associated with a shallow, marginal-marine depositional setting based on facies analysis and a pervasive brackish-water ichnofossil suite (Pemberton *et al.*, 1982). The ichnology of the Nauta system shows evidence of brackish-water to normal marine conditions (see below), but the degree of bioturbation is only locally pervasive. Other examples showing similar facies make up, and interpreted as shallow marginal marine deposits are reported from the Late Cretaceous Ipixuna Formation of north-eastern Brazil (Rossetti & Santos, 2003); the late Cenozoic of north-eastern Brazil (Rossetti, 2001); the Miocene Solimões Formation in Brazil (Hoorn, 1994b; Räsänen *et al.*, 1995; Gingras

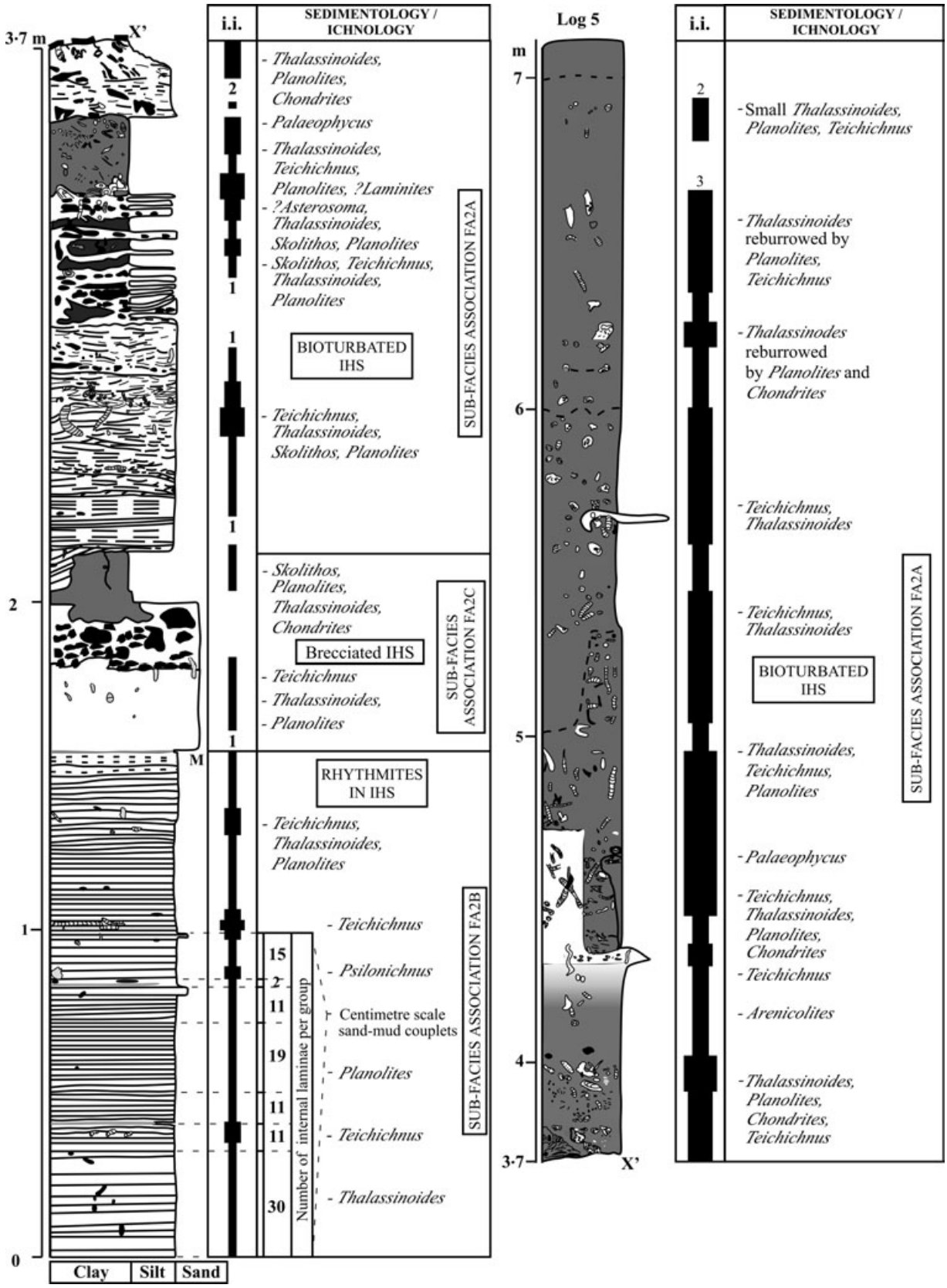

Fig. 14. Graphic log for interval 5 of Section 4. See Fig. 12 for location. Note counts over lower metre of log, where there are groups of 30 to 11 laminae that could be attributed to monthly to semi-monthly cyclicity. See Fig. 5 for key to legend and ichnofabric index (i.i.).

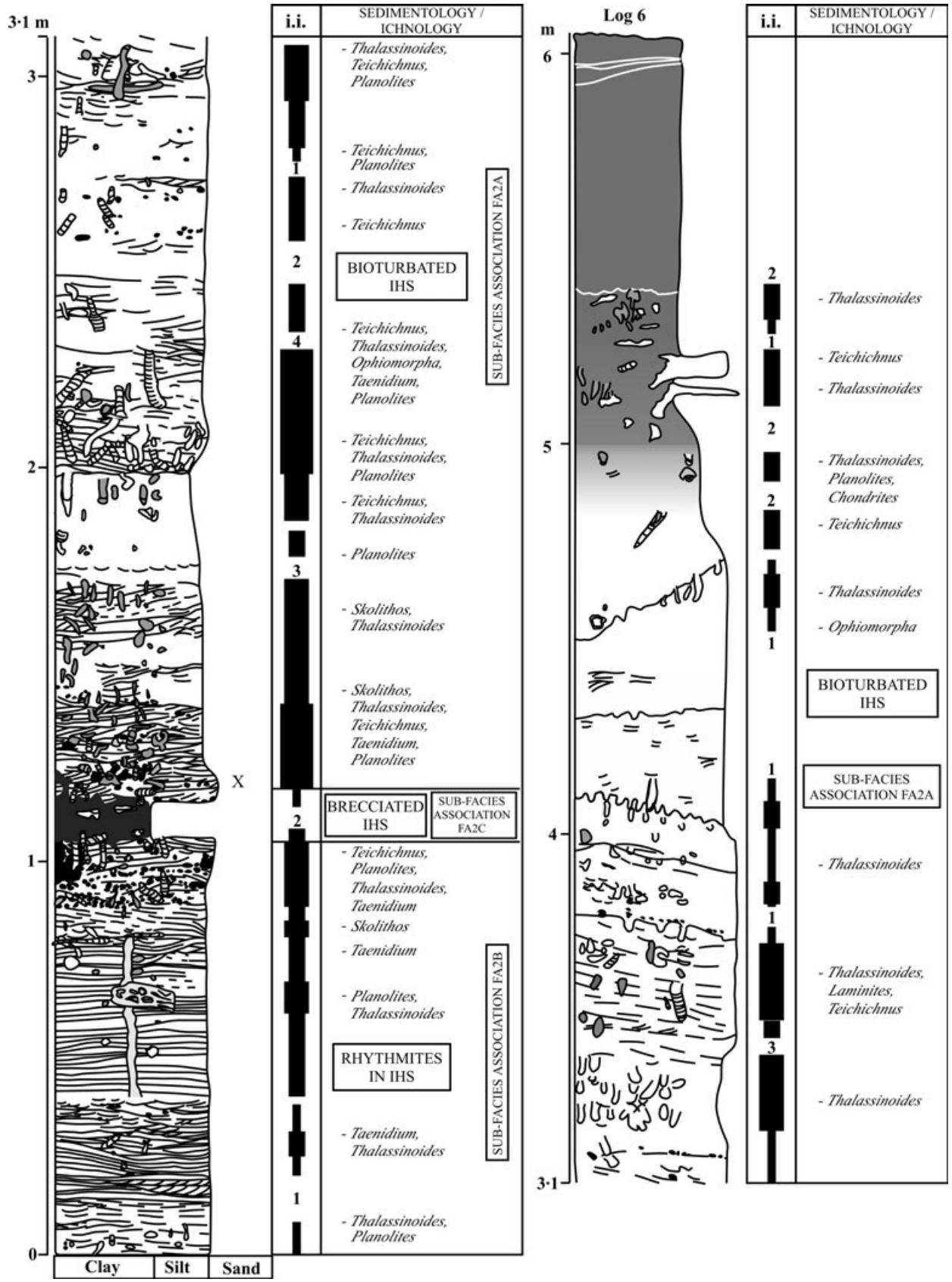

Fig. 15. Graphic log for interval 6 of Section 4. See Fig. 12 for location and Fig. 5 for key to legend and ichnofabric index (i.i.).

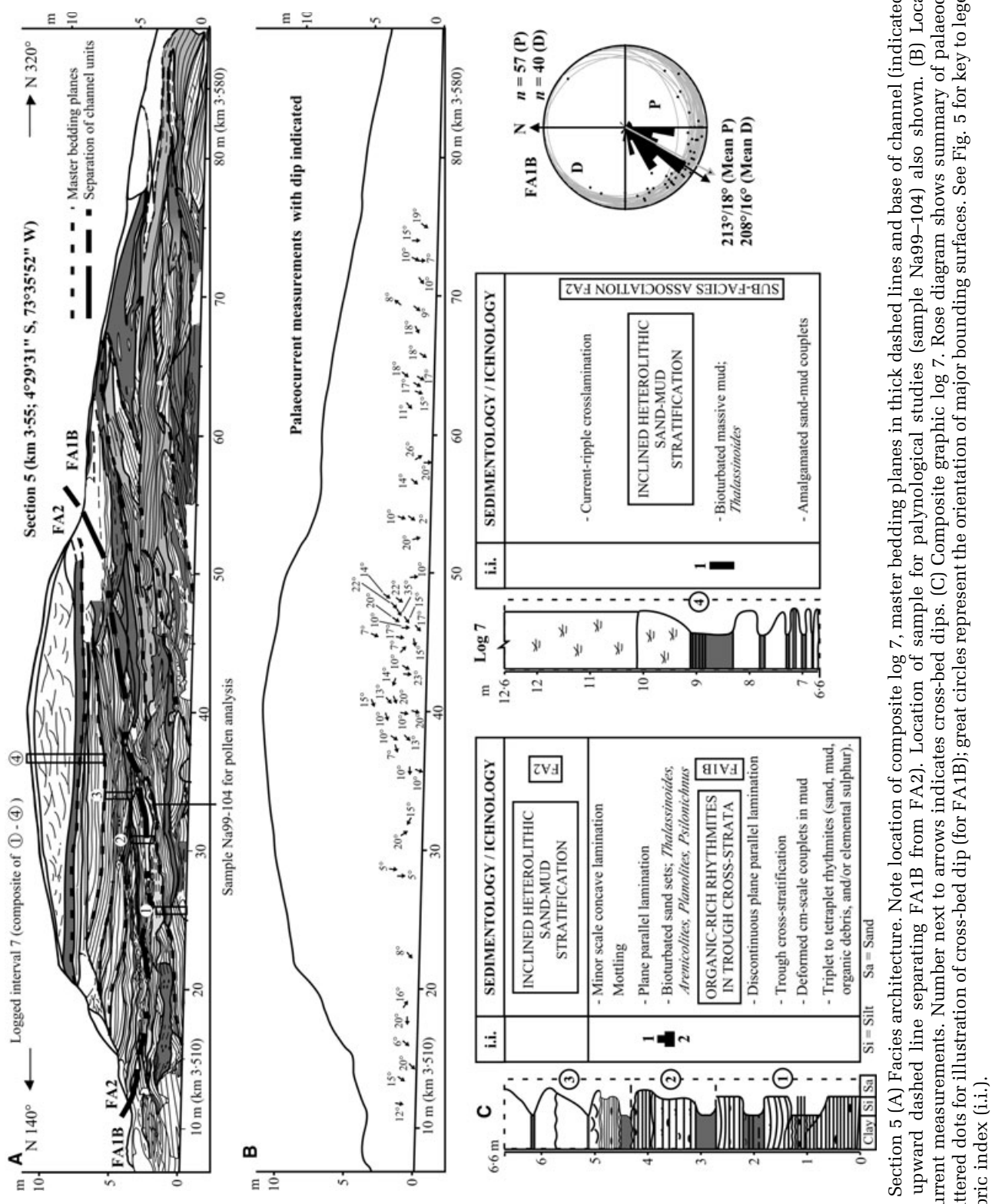

Fig. 16. Section 5 (A) Facies architecture. Note location of composite log 7, master bedding planes in thick dashed lines and base of channel (indicated by the concave upward dashed line separating FA1B from FA2). Location of sample for palynological studies (sample Na99–104) also shown. (B) Location of palaeocurrent measurements. Number next to arrows indicates cross-bed dips. (C) Composite graphic log 7. Rose diagram shows summary of palaeocurrents with scattered dots for illustration of cross-bed dip (for FA1B); great circles represent the orientation of major bounding surfaces. See Fig. 5 for key to legend and ichnofabric index (i.i.).

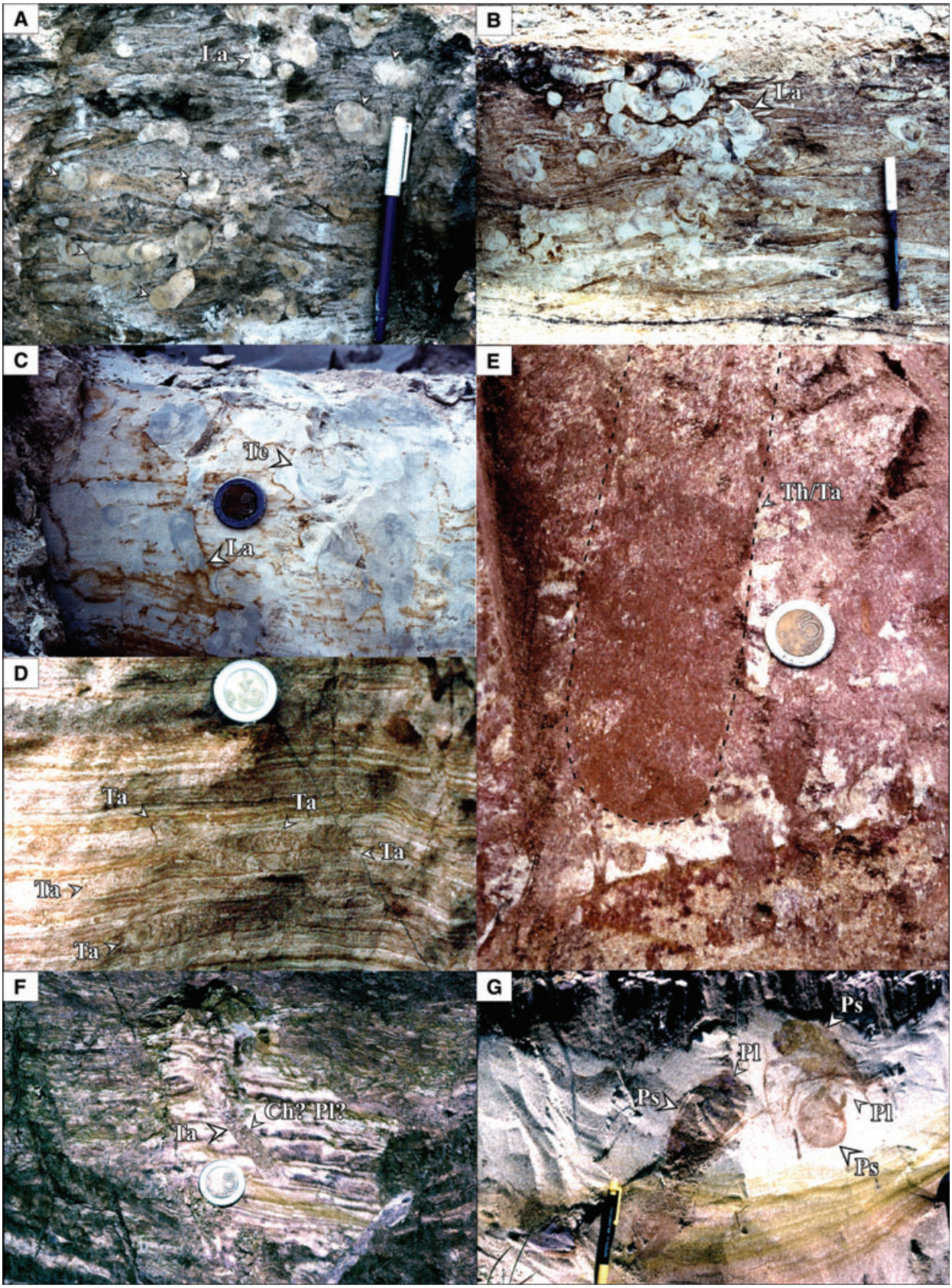
A
La
B
La
C
Tc
La
D
Ta
Ta
Ta
Ta
Ta
E
Th/Ta
F
Ch? Pl?
Ta
G
Ps
Pl
Ps
Pl
Ps

et al., 2002a); the late Early to early Late Miocene Pebas Formation in Peru (Räsänen *et al.*, 1998; Gingras *et al.*, 2002b); the Pleistocene deposits of Willapa Bay (Clifton, 1982) and the modern deltaic deposits of the Han River in Korea (Choi *et al.*, 2004).

Evidence for tidal influence

Primary physical sedimentary structures support a tidal influence in the Nauta channel complex. Tidal influence is revealed by the millimetre and centimetre-scale cyclical arrangement of the rhythmites from all three facies associations. Each of the millimetre-scale doublets, triplets or tetraplets observed are interpreted as flood–ebb tidal cycles. The double mud drapes documented within some of the flood–ebb cycles, separating a thicker sand lamina from a thinner one, imply a strong asymmetrical tide or a weak subordinate current (Nio & Yang, 1991). Similar doublet to tetraplet combinations deposited during flood–ebb tidal cycles have been reported from inner-estuary mud flats in the Cobequid Bay–Salmon River estuary (Dalrymple *et al.*, 1991). The *ca* 7 cm thick bundles in the Nauta rhythmites containing 12 to 14 mm scale thin laminae and one thick sand layer are interpreted as representing amalgamated neap–spring tidal cycles (cf. Räsänen *et al.*, 1998); the thick sand layer representing deposition during spring tides and the thinner laminae corresponding to neap tides (Fig. 4F). The alternating deformed and non-deformed organic-rich rhythmites may also record neap–spring cycles based on their similarity in thickness with the aforementioned bundles, and on their internal millimetre-scale lamination delineating flood–ebb tidal cycles. An example of deformed and non-deformed couplets has been reported from the inner-estuary mud flats in the Cobequid Bay–Salmon River estuary, though there the cycles are 5–30 cm in thickness and clearly represent annual deposits (cf. Dalrymple *et al.*, 1991).

Other characteristic tidal features in the Nauta complex include mud-draped trough cross-stratification and ripple lamination (e.g. Fig. 4C), millimetre-scale rhythmites without clear evidence of tidal cyclicity, flaser and lenticular bedding, IHS (e.g. Fig. 4B), intraformational rip up mud clasts (Fig. 4H) and bi-directional palaeocurrents (Fig. 7; Reineck & Wunderlich, 1968; Terwindt & Breusers, 1972; Reineck & Singh, 1986). In addition, the micro-faults and soft-sediment deformation (observed within the Nauta deposits, e.g. see Fig. 4G) are common features in tidal flat environments (Clifton, 1982; Reineck & Singh, 1986). Moreover, sediment transport vectors at the different outcrops are characterized by polymodal palaeocurrent directions (Fig. 18), a complexity possibly related to local tidal transport asymmetry (Allen, 1991), although it could also be partly due to the sinuosity of the tidal channels (see above).

Evidence for seasonal deposition

The decimetre- and metre-scale sand–mud couplets in the Nauta channel complex could result from repetitive autocyclic changes (e.g. different current velocities, changes in the sedimentary input, the shifting of channels and shoals) and/or from long-term periodic climatic variations (e.g. annual changes in precipitation, temperature or wind direction) (Terwindt, 1975; Dalrymple *et al.*, 1991). A long-term control is likely for these couplets, because each couplet includes evidence for a number of neap–spring tidal cycles (see above) in their mud-dominated parts, implying several months of deposition. The sedimentology and ichnology of the Nauta decimetre-scale couplets are locally similar to the annual couplets documented by van Den Berg (1981) in subtidal abandoned channels in the Oosterschelde tidal inlet. These were described as 20–60 cm thick, sandy to muddy couplets. The Oosterschelde couplets were interpreted as seasonal beds representing high-energy winter-spring (sandy part) vs

Fig. 17. Selected pictures of brackish-water to normal marine ichnofabrics in the Nauta Formation. (A) *Laminites* (La)-dominated ichnofabric (FA2A at section 3) indicative of normal marine conditions. Close ups of La; probable burrow makers were heart urchins. See Table 3. Note arrows. Pen is *ca* 14 cm long (B) *Laminites* (La)-dominated ichnofabric (FA2A at section 3). Pen is *ca* 14 cm long (C) *Laminites* (La) and large crustacean-generated *Teichichnus* (Te). Coin is *ca* 2·5 cm in diameter. (D) Ta-dominated ichnofabric within rhythmites (FA2B at section 4). Coin is *ca* 2·2 cm in diameter. (E) Composite fabric of large *Thalassinoides* (Th) and *Taenidium* (Ta; FA3A at section 3). Ta is found also in freshwater facies (see Table 3). Coin is *ca* 2·5 cm in diameter. (F) Ta cross-cutting rhythmites (FA3A at Section 3). Ta is reburrowed by *Chondrites* (Ch?)/Pl?-like traces. Coin is *ca* 2·5 cm in diameter. (G) Large reddish mud-filled *Psilonichnus* (Ps) traces with some reburrowing by *Planolites* (Pl; see small arrows; FA2C at section 4) descending into whitish sand. Pen for scale.

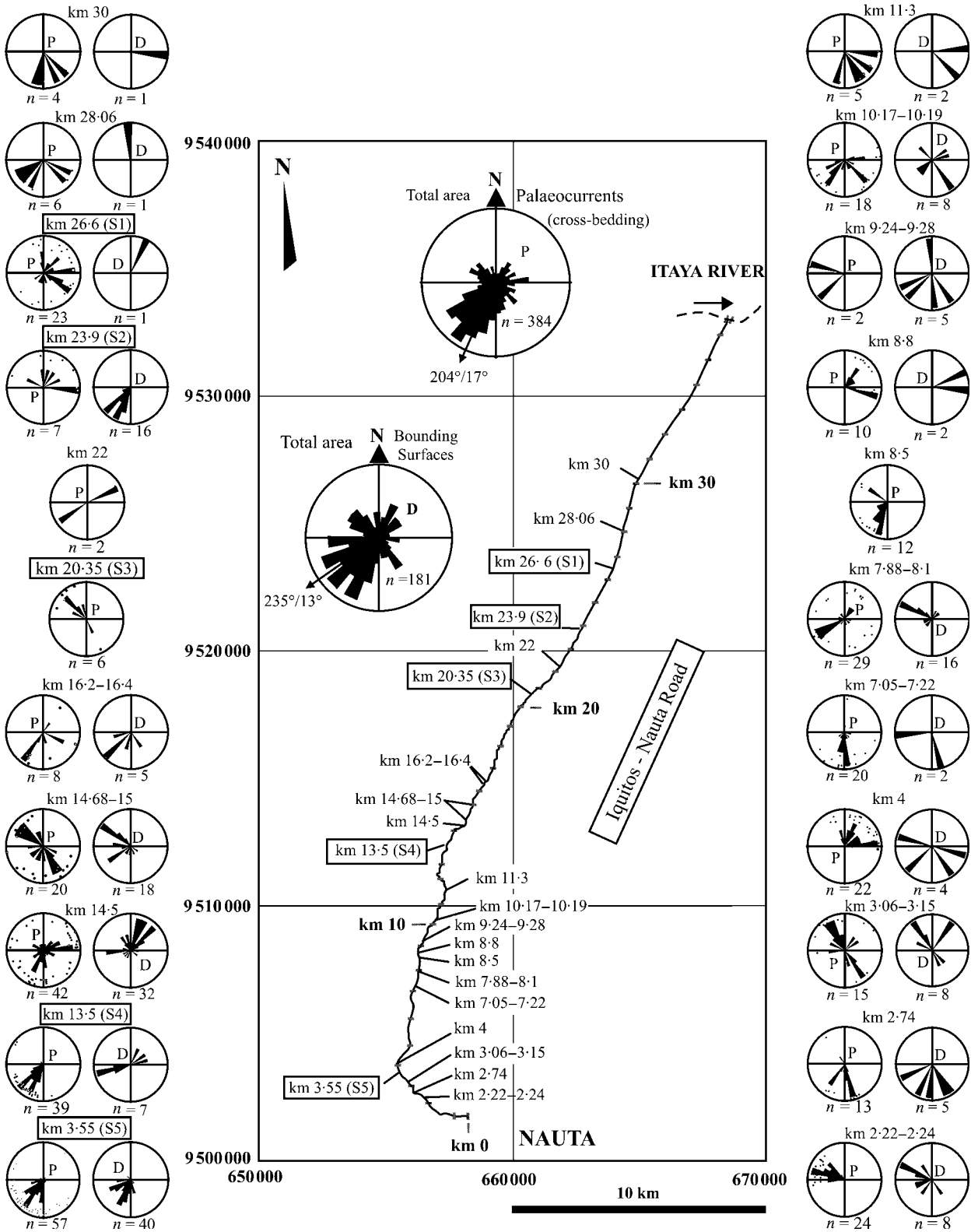

Fig. 18. Site by site rose diagrams with palaeocurrent (P) and bounding surface (D) orientations (dip direction, dip) measured along the last *ca* 40 km of the Iquitos–Nauta Road showing strong polymodality between sites. Two compound rose diagrams from the whole area depicting a dominant SW-oriented mode are presented in the centre of the figure. Sections 1 to 5 (S1–S5) from the present study. See Fig. 3A for location. Coordinates are in UTM projection.

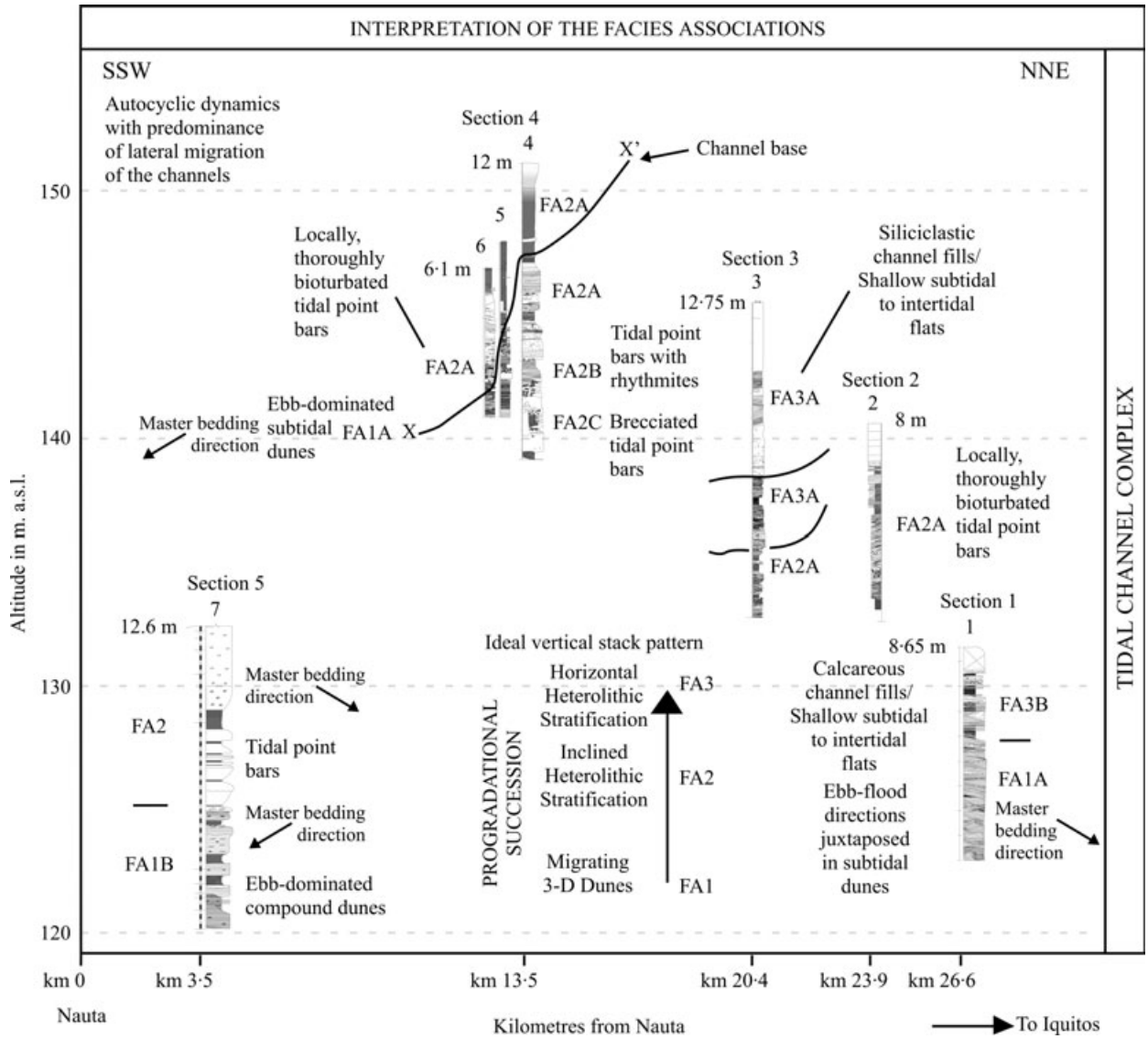

Fig. 19. Location of Sections 1–5 according to their relative altitude. Notice the identified facies associations (FA1–FA3) with their respective sub-facies (see text) and interpretation. See Fig. 5 for legend.

low-energy summer-fall (muddy part) sedimentation. The existence of a Miocene bi-seasonal annual cyclicity comparable to the modern wet vs. dry seasonal annual change in western Amazonia, demonstrated from molluscan growth increments (Kaandorp *et al.*, 2005), supports a bi-seasonally induced deposition for the Nauta beds. Thus, the sand-dominated parts in the decimetre-scale sand–mud couplets may represent sediment deposition during high-energy rainy seasons and the mud-dominated parts sedimentation during low-energy dry seasons. However, the thickness of annual cycles can overlap in scale with neap–spring tidal cycles, depending on the location (e.g. centimetre- to decimetre-scale neap–spring intertidal couplets vs. centimetre- to decimetre-scale annual supratidal couplets; Tessier, 1998).

Fan & Li (2002) interpreted centimetre- to decimetre-scale couplets from the intertidal mudflats of the Changjiang Estuary as storm vs. calm weather annual cycles. An annual interpretation seems plausible for the metre scale couplets in the Nauta complex, especially for those with brecciated mud. This is because at the beginning of each new rainy season, erosion by tidal currents and/or waves is enhanced and mud layers are easily reworked; at the end of the rainy season, the reworked mud clasts/blocks were redeposited as brecciated layers. The original mud

layers prior to erosion were deposited over several months; internally many of the brecciated mud blocks show several centimetre-scale cycles, interpreted herein as neap–spring tidal cycles (see above). Some of the mud brecciated layers may have also been caused by mud slides or storms.

The Nauta trace fossil ichnofabrics also support seasonal deposition (cf. Gingras *et al.*, 2002a,b). The Nauta succession is characterized by locally pervasively bioturbated sand-mud couplets, with bioturbation concentrated in the mud-dominated parts and continuing downwards into the sand-dominated parts (most traces in sand are mud-filled because burrowers carried the mud downwards). This alternation between bioturbated and less to non-bioturbated sets, usually observed in single IHS sets, may have a seasonal origin because colonization by burrowing organisms is controlled by larval recruitment, which is commonly a seasonal or annual phenomenon (Gingras *et al.*, 2002a).

Biogenic evidence for a marginal marine environment

The overall low diversity and trophic–generalist behaviour of the trace fossils in the Nauta Formation is consistent with deposition under brackish-water conditions (cf. Pemberton *et al.*, 1982; see also Gingras *et al.*, 2002a,b), with some local periods of normal marine conditions exemplified by the presence of *Laminites*, a burrow most probably made by spatangoid echinoids (Plaziat & Mahmoudi, 1988). The main trace fossils and trace fossil associations in the Nauta system and their palaeo-environmental significance are summarized in Table 3.

FA1 contains the most saline assemblage (i.e. *Skolithos*, *Thalassinoides*, and *Teichichnus* with rarer, *Taenidium*, *Planolites*, *Scolicia*, *Ophiomorpha* and *Chondrites*). This diversity is attributed to the consistent presence of a salt-water wedge in the lower part the channels. In contrast, FA2 contains lower diversity trace-fossil assemblages: particularly the *Planolites – Chondrites* association in mud beds, and *Skolithos – Planolites* or *Laminites – Thalassinoides* associations in sand beds. The lower diversity assemblages may reflect tidal or seasonal variations in salinity above the salt-water wedge. Finally, FA3 is dominated by *Taenidium*, but includes a variety of trace fossils (e.g. *Planolites*, *Chondrites*, *Arenicolites*, *Psilonichnus*, and rare *Rhizocorallium*). This ethologically broad assemblage of trace fossils is consistent with tidal flats (Gingras *et al.*, 1999). However, *Taenidium* most likely represents a shift to subaerial exposed sediment and final shoaling to a supratidal flat.

Two ichnofacies predominate: (i) *Skolithos*- and *Thalassinoides*-dominated assemblages that represent a low-diversity (stressed) *Skolithos* ichnofacies, which is mostly present in sandy strata; and, (ii) *Laminites*-, *Taenidium*- and *Planolites*-dominated fabrics that are taken to represent an impoverished *Cruziana* ichnofacies that occurs in low-energy sands (normally burrowed by *Laminites*) and muddy beds (Bromley & Frey, 1974; Bromley & Ekdale, 1984; Frey & Bromley, 1985). Moreover, a mixed *Skolithos–Cruziana* ichnofacies is locally dominant, particularly in the IHS of FA2. Both ichnofacies, and particularly their admixture, are associated with estuarine settings (Pemberton *et al.*, 1992; Beynon, 1994; Buatois *et al.*, 1998) and brackish-water deltaic settings (see McIlroy, 2004 and references therein).

The infauna demonstrates a strong response to substrate lithology. The ichnoassemblages within sand imply well-oxygenated environments with a reasonable nutrient supply (Fig. 17). Organisms had to be able to respond rapidly to potentially stressful conditions (e.g. fluctuating salinity, shifting substrates). In contrast, the bioturbated, muddy bedsets represent deposition during lower energy periods; the mud beds drape troughs and sand–mud couplets in all facies associations. Colonization of the muddy sediments was facilitated by the presence of a stable sediment–water interface.

The overall high degree of bioturbation within mud at the base of the IHS sand-mud successions (e.g. FA2A at base of log in Fig. 9) and in mud drapes (e.g. very high abundance of diminutive trace fossils in FA1A), probably indicates that initially, mud sedimentation rates were generally low and salinity and oxygen levels were stable. The diminutive trace fossils probably represent the work of threadworms similar to the modern capitellid *Heteromastus*. Threadworms seldom are present in such abundance in continental systems. Fluctuations in salinity and oxygen-content could explain the general abundance patterns or local lack of trace fossils (Clifton & Phillips, 1980; Gingras *et al.*, 1999). The upward decrease in the size of the traces in FA2 and FA3 (see the upper 5 m of the log in Fig. 11) probably reflects a salinity stress, which in this case means lower salinity, likely due to salinity stratification (Pemberton *et al.*, 1982). Channel bottoms may have had the least fluctuating conditions (base of

Table 3. Palaeoenvironmental significance of main ichnological elements from the Nauta Formation based on their known general characteristics and distribution.

Trace fossils or trace fossil associations	General characteristics and typical environments
Skolithos	Common in depositional environments dominated by shifting substrates and moderately high hydraulic energy (Seilacher, 1963, 1967). For those reasons, this trace is common in shoreface and tidal channel deposits. Moreover, it is most commonly associated with marine to brackish water (i.e. mesohaline to marine salinity)
Thalassinoides	Common in shifting sediments; however, it is usually associated with somewhat lower energy conditions than *Skolithos*. It is also most commonly associated with marine to brackish water (i.e. mesohaline to marine salinity)
Scolicia group: Variant *Laminites*	Almost exclusively generated by spatangoid echinoids (Plaziat & Mahmoudi, 1988). The presence of this group in the Nauta deposits is particularly interesting because it has only been observed in water where salinity is quite high (>20 or 25 ppt.), ranging from deep marine to shallow marine settings (Bromley & Asgaard, 1975; Smith & Crimes, 1983; Fu & Werner, 2000). Particularly, the presence of *Laminites* in the Nauta system supports marginal marine conditions (e.g. Gingras *et al.*, 2002b)
Thalassinoides –*Scolicia*	Apparently developed in a shifting substrate that suffered moderate to rare sedimentation events. Both traces indicate relatively high oxygen levels, as they dominate only in normally oxygenated substrates
Rhizocorallium	Commonly characterizes low-energy to quiet environments where organisms could adjust their feeding activities repetitively (Seilacher, 1967).
Chondrites	Generally taken to indicate anoxic conditions (Bromley & Ekdale, 1984). Because this trace can be associated with low-oxygen conditions, it is a common element of ingression and maximum flooding surfaces. It has only been observed from marginal-marine to brackish-water settings
Taenidium	Attributed to the activities of worms, crustaceans, and insect larvae, hence indicating mostly freshwater conditions or low-salinity settings. However, it has also been observed in marine waters
Taenidium –*Chondrites* and -*Planolites* –*Chondrites*	In the Nauta system, these traces (i.e. *Taenidium* and *Planolites*) are locally reburrowed by *Chondrites*. Because *Chondrites* indicates low-oxygen levels and has only been reported from marine to brackish-water settings, these associations suggest oxygen-depleted, near-shore environments
Teichichnus	Most commonly interpreted to represent the response of burrowing organisms to rapid sediment accumulation (Pemberton *et al.*, 1992). It has also been linked to resource-rich sediment in environments dominated by shifting substrates (Zonneveld *et al.*, 2001)
Psilonichnus	The most probable tracemakers for these traces are mantis shrimps, lobsters or possibly crabs, which commonly live in a wide range of tidal subenvironments (Gingras *et al.*, 2000)
Planolites	Actively backfilled burrows built by a mobile deposit feeder, which ingest the sediments and hence modify them biochemically and physically (Pemberton & Frey, 1982)

FA2) as opposed to the upper levels (top of FA2 and FA3).

The Nauta *Laminites*-dominated associations (Fig. 17A and B) are similar to those originally described by Reineck & Singh (1986) from tidal environments along the northwest coast of Germany and by van Den Berg (1981) from the Oosterschelde annual couplets (compare Fig. 9 of van Den Berg (1981) with the lowermost 2 m in Figs 11 and 17A,B in this paper). These associations give strong evidence of normal marine conditions because the *Laminites* behaviour has only been reported from environments characterized by polyhaline and marine waters (*ca* 30 psu; Bromley & Asgaard, 1975; Smith & Crimes, 1983; Plaziat & Mahmoudi, 1988; Fu & Werner, 2000; Gingras *et al.*, 2002b; Table 3). Other similar marginal-marine ichnofossil assemblages have been reported, for instance, from the Pleistocene deposits of Willapa Bay, Washington (Gingras *et al.*, 1999, 2000), Middle and Late Miocene deposits of the Solimões Formation (Gingras *et al.*, 2002a), the late Early to early Late Miocene Pebas Formation (e.g. Räsänen *et al.*, 1998; Gingras *et al.*, 2002b), and the Late Cretaceous Ipixuna Formation of northeastern Brazil (Rossetti & Santos, 2003). Finally, the Nauta palynological data (Table 4) further support a marginal marine setting because mangrove or mangrove-related systems commonly develop in brackish-water conditions (e.g. Lorente, 1986; Hoorn, 1994c).

Table 4. All palynomorph species with their number of grains, percentage distribution and concentration from section 5, sample Na-99–104 (see Fig. 16A for location).

Item no. of species	ID code	Palynomorphs (47 species)	No. of grains	Percentage	Concentration (grains cm^{-3})	Ecological affinity
1	3109	*Psilatricolporites maculosus*	11	3·23	80	Assemblage 1 (15·54%)
2	3117	*Retitricolpites simplex* type 01	25	7·33	250	related to mangrove
2	3110	*Retitricolpites simplex* type 02	5	1·47	40	environments
3	3126	*Retitricolporites* sp. type 01	3	0·88	20	(cf. Rull, 2001).
3	3118	*Retitricolporites* sp. type 03	3	0·88	20	
4	3107	*Zonocostites* sp. type 02	6	1·76	50	
5	3065	*Cuphea* type 01	1	0·29	10	Assemblage 2 (18·18%)
6	3019	*Cyperaceapollis*	7	2·05	50+	related to herbaceous
7	3074	*Deltoidospora sp.* (Spore)	1	0·29	10	back-mangrove swamp
8	3115	*Laevigatosporites sp.* (Spore)	1	0·29	10	environments. These
9	3007	*Monoporites annulatus*	7	2·05	50+	species include flora
10	3022	*Perisyncolporites pokornyi* Type 01	4	1·17	30	resistant to low salinity to freshwater conditions.
11	3014	*Psilaperiporites minimus*	1	0·29	10	
12	3116	*Psilatricolporites operculatus* Type 01	11	3·23	80	
12	3121	*Psilatricolporites operculatus* Type 02	8	2·35	60+	
13	3039	*Psilatricolporites triangularis* Type 01	20	5·87	200	
14	3046	*Syncolporites incomptus*	1	0·29	10	
15	3026	*Clavainaperturites microclavatus*	2	0·59	10+	Assemblage 3 (14·37%)
16	3112	*Crototricolpites sp.* Type 02	14	4·11	140	related to rainforest or
17	3111	*Cupanieidites sp.*	4	1·17	30	floodplain environments.
18	3106	*Echiperiporites stelae*	2	0·59	10+	
19	3025	*Heterocolpites incomptus*	11	3·23	80	
20	3003	*Myrtaceidites sp.* Type 01	3	0·88	20	
20	3129	*Myrtaceidites sp.* Type 2	3	0·88	20	
21	3070	*Proteacidites sp.* Type 2	4	1·17	30	
22	3011	*Psiladiporites redundantes*	2	0·59	10+	
23	3133	*Psilatricolporites labiatus* Type 03	2	0·59	10+	
24	3002	*Scabratriporites moderatus* Type 03	2	0·59	10+	
25	3119	*Equimorphomonocolpites solitarius*	2	0·59	10+	Assemblage 4 (2·93%) related to palm swamp
26	3035	*Mauritiidites sp.*	3	0·88	20	environments.
27	3044	*Psilamonocolpites sp.*	2	0·59	10+	
28	3050	*Retimonocolpites maximus*	3	0·88	20	
29	3134	*Cricotrisporites sp.*	2	0·59	10+	Assemblage 5 (48·97%);
16	3064	*Crototricolpites sp.* Type 01	2	0·59	10+	species with unknown
30	3135	*Cyatheacidites annulatus*	2	0·59	10+	botanical affinity and
31	3123	*Matonisporites sp.*(Spore)	2	0·59	10+	with unknown or a wide
32	3056	*Psilatricolpites anconis*	13	3·81	100	range of environmental
33	3055	*Psilatricolporites corstanjei*	2	0·59	10+	conditions.
34	3009	*Psilatricolporites exiguos*	4	1·17	30	
35	3122	*Psilatricolporites garzonii*	4	1·17	30	
36	3103	*Psilatricolporites minutus*	3	0·88	20	
37	3136	*Psilatricolporites silvaticus*	2	0·59	10+	
38	3090	*Psilatricolporites varius* Type 02	87	25·51	840	
39	3073	*Psilatricolporites crassoexinatus* Type 01	2	0·59	10+	
39	3113	*Psilatricolporites crassoexinatus* Type 02	8	2·35	60+	
40	3114	*Retibrevitricolporites grandis*	9	2·64	70	
41	3120	*Retistephanocolpites sp.* Type 01	2	0·59	10+	

Table 4. (Continued.)

Item no. of species	ID code	Palynomorphs (47 species)	No. of grains	Percentage	Concentration (grains cm^{-3})	Ecological affinity
41	3127	*Retistephanocolpites sp.* Type 02	2	0·59	10+	
41	3130	*Retistephanocolpites sp.* Type 03	2	0·59	10+	
42	3069	*Retitricolpites colpiconstrictus*	4	1·17	30	
43	3108	*Retitricolporites kaarsini*	3	0·88	20	
44	3061	*Retitricolporites leticianus*	2	0·59	10+	
45	3100	*Retitricolporites milnei*	5	1·47	40	
46	3132	*Retitricolporites pigmaeus*	2	0·59	10+	
47	3043	*Scabratriporites sp.* Type 02	3	0·88	20	
		Total palynomorphs	341	100·0		

DISCUSSION

Palaeo-environment of the Nauta Formation

The Late Miocene Nauta deposits have been previously interpreted as tidally influenced estuarine units (Räsänen *et al.*, 1998) and as fluvially dominated successions (Martínez-V. *et al.*, 1999; Sánchez-F. *et al.*, 1999). Those interpretations did not, however, include a detailed documentation of the ichnology. The ichnological evidence reported herein strongly supports a marginal marine origin for the Nauta strata (see above); trace fossil assemblages are consistent with overall brackish to, locally, normal marine conditions during deposition. Furthermore, recent ichnological studies elsewhere in north-western Amazonia support the interpretation of estuarine to marginal marine environments during the Miocene in this region (e.g. Gingras *et al.*, 2002a,b; Hovikoski *et al.*, 2005). However, brackish-water depositional conditions are common not only in estuarine, but also in deltaic settings, and particularly in tide-dominated deltas (see e.g. McIlroy, 2004).

The tide-influenced Nauta channel complex is characterized by facies associations usually found in the inner part or central, low-energy, meandering zone of tide-dominated estuaries, such as the Cobequid Bay–Salmon River macrotidal estuary (see e.g. Dalrymple *et al.*, 1991, 1992; Dalrymple, 1992) or in the inner part and/or the abandoned channels in delta plains of tide-dominated deltas, which are usually subject to marine erosion after abandonment, such as the macrotidal Fly River and Han River deltas (see e.g. Dalrymple *et al.*, 2003; Choi *et al.*, 2004; McIlroy, 2004). A bay-margin setting is also plausible for the Nauta Formation, because the abundance of trace fossils suggests a sheltered environment, whereas the low diversity, brackish-water assemblages rule out an open-sea, bay-mouth system. Hence, the Nauta Formation is attributed to a mixed-energy, sub-aqueous setting in the transition from a marginal marine to a brackish-water embayed coastal environment (cf. the coastal classification prism of Dalrymple *et al.*, 1992).

Tidal effects were moderate-to-high in the channel complex, whereas wave influence was negligible. River influence in general was not negligible as depositional rates were high. The generally high depositional rates caused the easy deformation of the deposits, partly by sliding on the inclined surfaces (of IHS), partly due to erosion and reworking during the initiation of the sand deposition.

There is no conclusive evidence to further constrain the Nauta system as estuarine or deltaic, but the transitional change from the finer-grained shoreface parasequences of the Pebas Formation below, to the coarser-grained channel complex of the Nauta Formation indicates progradation and is consistent with a deltaic setting. Consequently, the complex network of meandering brackish-water tidal channels in the Nauta Formation could have developed in an abandoned delta plain sub-environment, whereby reworking by tidal currents was important (Fig. 20). A marginal marine setting is further supported by the comparatively less stressed (i.e. salinity levels were probably higher and/or more stable) ichnofossil assemblages (e.g. *Scolicia*-dominated ichnofabrics) in the Nauta Formation compared to the underlying Pebas Formation (Gingras *et al.*, 2002b). The palynological evidence (Table 4) also suggests a stronger marine influence in the Nauta Formation than in the uppermost beds of the Pebas Formation (see Hoorn, 1994c; Rebata-H. *et al.*, 2006).

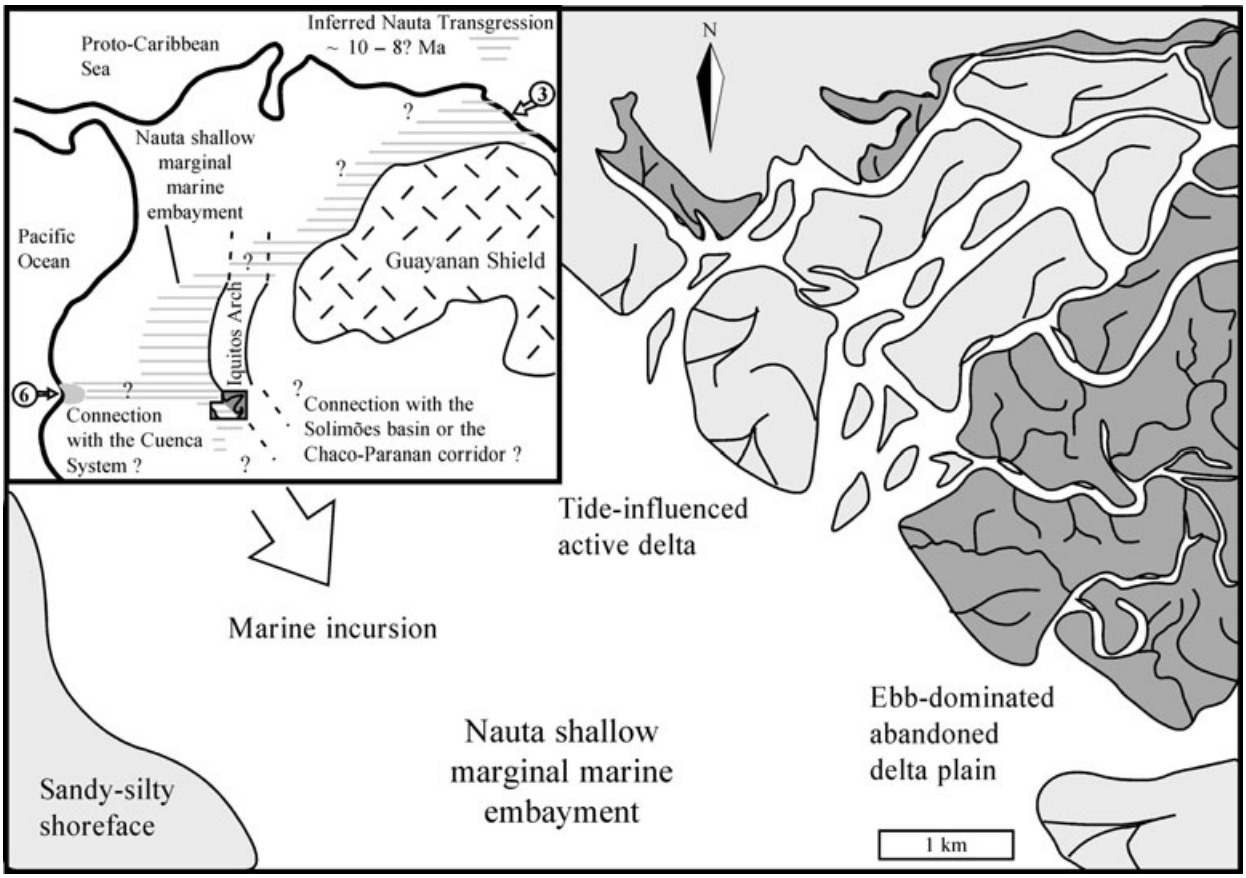

Fig. 20. Palaeogeographic reconstruction of the study area. The system is envisioned as a narrow, shallow, marginal marine embayment where ebb-dominated tidal channel complexes developed in the inactive part of delta plains. Note inferred location of the system in northern South America during the Late Miocene (inset), where two possible pathways for the Tortonian Nauta transgression are indicated with light grey dashed lines: one through portal 3 (modified after Vonhof *et al.*, 1998) and one through portal 6 (modified after Nuttall, 1990; Steinmann *et al.*, 1999; Hungerbühler *et al.*, 2002). A connection with the Solimões Basin or Chaco-Paranan corridor Late Miocene deposits is also quite plausible.

Palaeogeography

The palaeogeographic reconstruction of the Nauta system presented in Fig. 20 depicts a NE–SW-oriented, tidally influenced channel complex located in the brackish-water portion of a delta plain, within a shallow epicontinental embayment. As the Nauta complex is located at the eastern margin of the Marañón foreland sub-basin, the local sediment input to the embayment probably came from the uplifting forebulge, represented by the Iquitos Arch (cf. Roddaz *et al.*, 2005) which acted to control the position of the palaeo-coast line. Based on the position and orientation of the palaeo-coast line and the SW-preferred orientation of palaeocurrents (Fig. 18), the Nauta tidal channels are inferred to have been ebb-dominated, with seasonal reinforcement of the ebb-tidal currents by river discharge. This scenario further supports a deltaic setting for the Nauta Formation (see above). The position and character of the Nauta channel complex in the embayment help refine the wider palaeogeographic evolution of northern South America prior to continentalization and establishment of the Amazon River system (Hoorn, 1993a,b, 1994a,b,c; Cooper *et al.*, 1995; Hoorn *et al.*, 1995; Guerrero, 1997; Lovejoy *et al.*, 1998; Lundberg *et al.*, 1998; Roddaz *et al.*, 2005). Marine influence in the Nauta Formation reflects late incursions of the sea, possibly from the Proto-Caribbean Sea through portal 3 and/or from the Pacific Ocean through portal 6 (see e.g. Nuttall, 1990; Hoorn, 1994c; Vonhof *et al.*, 1998; Steinmann *et al.*, 1999; Hungerbühler *et al.*, 2002; Figs 1 and 20). The link with portal 3 is suggested by palynological evidence from the Middle to Late Miocene Apaporis sand unit (Colombia) indicating the presence of mangrove forests fringing the Guayanan Shield during that

time (Hoorn, 1994c). Evidence of deltaic marginal marine sedimentation through portal 6, across the Cuenca area in Ecuador, is mainly recorded in the Middle to Late Miocene (*ca* 13·9–9·5 Ma) Loyola, Azogues and Mangán formations, where brackish water to marine flora and fauna have been documented (Steinmann *et al.*, 1999; Hungerbühler *et al.*, 2002). Portals 1 and 2 were presumably already closed by the time the Nauta system developed (Hoorn, 1993a; Cooper *et al.*, 1995; Hoorn *et al.*, 1995; Guerrero, 1997). Further studies are required to establish the relationship between the Nauta Formation and its equivalents in Brazil across the Solimões, Amazonas and Foz do Amazonas basins (Fig. 1).

The Nauta Formation is probably linked with tidally influenced, *ca* 9 Ma old deposits from the Ipururo and Madre de Dios formations in the Madre de Dios Basin (cf. Hovikoski *et al.*, 2005), *ca* 10–8 Ma old deposits from the Solimões Formation in the area between the Madre de Dios, Acre and Solimões (sub)basins (cf., Räsänen *et al.*, 1995), Late Miocene deposits from the Cobija Formation in the Beni Plain basin (cf. Räsänen *et al.*, 1995) and Upper Miocene deposits from the Ipururo Formation in the Huallaga Basin (cf. Hermoza *et al.*, 2005) (Fig. 1).

The northernmost tip of the *ca* 10–8 Ma old, Paranan-Entrerriense system, which covered most of the Chaco-Paranan corridor along Bolivia, Paraguay and Argentina, is reportedly represented by the marginal marine deposits of the Middle to Late Miocene Yecua Formation in Bolivia (Marshall & Sempere, 1991; Marshall *et al.*, 1993; Hulka *et al.*, 2006; see also Boltovskoy, 1991; Räsänen *et al.*, 1995; Marengo, 2000), which may also be linked with the Nauta system.

CONCLUSIONS

The Nauta Formation, exposed in the eastern margin of the Marañón foreland sub-basin, Peru, is characterized by Upper Miocene, unlithified, heterolithic deposits mostly composed of fine-grained bluish grey to variegated sand and mud, with an overall coarser grain size than the underlying Pebas Formation. The Nauta sediments represent a system of tidal-channel deposits that were most probably ebb-dominated and developed on the inactive portions of delta plains fringing a shallow brackish-water embayment where normal marine salinity conditions occurred episodically.

The tidal channel deposits include subtidal compound dunes, laterally accreting bars and shallow subtidal to intertidal channel fills. The abundance of cross sections with high-angle IHS, exposed along a NE–SW transect parallel to the dominant palaeocurrent, suggests the tidal channels were curved rather than straight.

Two orders of minor-scale cyclicity have been observed in thinly laminated tidal rhythmites, specially within the IHS: (i) a centimetre-scale thickness variation in sand-dominated to mud-dominated couplets depicting neap–spring tidal cycles (cf. Räsänen *et al.*, 1998); and superimposed (ii) millimetre-scale sand-mud couplets correlated with flood–ebb tidal cycles. Additional features characteristic, though not diagnostic, of tidal sedimentation include mud drapes in trough cross-stratified beds, flaser and lenticular bedding, IHS, rip-up mud clasts, millimetre-scale rhythmites without evidence of tidal cyclicity and bidirectional palaeocurrents.

Two styles of major-scale cyclicity have been documented: (i) decimetre-scale sand to mud couplets, the muddy parts of which include several neap–spring tidal cycles, are interpreted as annual cycles representing deposition during rainy and dry seasons, respectively; and (ii) metre-scale sand-dominated to mud-brecciated couplets, interpreted also as annual cycles, that most likely illustrate the reworking by strong currents or the sliding of partially consolidated mud at the beginning of the rainy seasons.

Both the ichnology and palynology of the tidal channel deposits support a marginal marine depositional environment. Trace fossil associations show low-diversity and a trophic-generalist behaviour characteristic of brackish-water environments. The associations are representative of impoverished *Skolithos*, *Cruziana*, and mixed *Skolithos–Cruziana* ichnofacies. Burrowing by infaunal echinoids indicates that locally normal marine salinity prevailed in the shallow embayment. The palynological content is characterized by a high diversity and a low concentration of well-preserved fossil pollen and spores. The palynological assemblages are indicative of coastal plain environments fringed by mangrove forests, herbaceous back-mangrove swamps, rainforests, floodplains and palm swamps.

Although it has been previously thought that marine influence in Northwestern Amazonia ended during the Serravallian, the shallow brackish-water to locally, normal marine tidal channel network documented herein indicates that areas

around latitude 4°30′ S had a marine connection during the Tortonian (*ca* 10–8 Ma).

ACKNOWLEDGEMENTS

The authors are grateful for funding from the Academy of Finland through FIBRE and the Ministry of Education of Finland through the Graduate School in Environmental Geology of the University of Turku. We thank Edward Córdova Romero and Elba María Ponce Arias for capable field assistance, the Geological Survey of Peru (INGEMMET) for logistic support, Dr. Georg Irion for the XRD-clay mineralogic analyses and fruitful discussions, Frank Wesselingh and Jussi Hovikoski for constructive comments, and Dr. Carina Hoorn for advice about the palynological interpretations. We gratefully acknowledge Dr. Robert W. Dalrymple and Dr. Peter Haughton for their careful reviews, valuable comments and thorough editing which helped to substantially improve this paper.

REFERENCES

Allen, J.R.L. (1980) Sand waves: a model of origin and internal structure. *Sed. Geol.*, **26,** 281–328.

Allen, G.P. (1991) Sedimentary processes and facies in the Gironde estuary: a recent model for macrotidal estuarine systems. In: *Clastic Tidal Sedimentology* (Eds D.G. Smith, G.E. Reinson, B.A. Zaitlin and R.A. Rahmani), *Can. Soc. Petrol. Geol. Mem.*, **16,** 29–40.

Beynon, B.M. (1994) Sedimentology and depositional history of the McMurray Formation and Wabiskaw Member, Northeastern Alberta. In: *C.S.P.G. Manville Core Conference* (Eds S.G. Pemberton, D.P. James and D.M. Wightman), pp. 245–277. Can. Soc. Petrol. Geol. Exploration Update 1994, Calgary, Alberta.

Boeger, W.A. and **Kritsky, D.C.** (2003) Parasites, fossils and geologic history: historical biogeography of the South American freshwater croakers, *Plagioscion* spp. (Teleostei, Sciaenidae). *Zoologica Scripta*, **32,** 3–11.

Boltovskoy, E. (1991) Ihering's hypothesis in the light of foraminiferological data. *Lethaia*, **24,** 191–198.

Bromley, R.G. and **Asgaard, U.** (1975) Sediment structures produced by a spatangoid echinoid: a problem of preservation. *Bull. Geol. Soc. Denmark*, **24,** 261–281.

Bromley, R.G. and **Ekdale, A.A.** (1984) *Chondrites*: a trace fossil indicator of anoxia in sediments. *Science*, **224,** 872–874.

Bromley, R.G. and **Frey, R.W.** (1974) Re-description of the trace fossil *Gyrolithes* and taxonomic evaluation of *Thalassinoides*, *Ophiomorpha* and *Spongeliomorpha*. *Bull. Geol. Soc. Denmark*, **23,** 311–335.

Buatois, L.A., Mangano, M.G., Maples, C.G. and **Lanier, W.P.** (1998) Allostratigraphic and sedimentologic applications of trace fossils to the study of incised estuarine valleys: an example from the Virgilian Tonganoxie Sandstone Member of Eastern Kansas. *Curr. Res. Earth Sci. Bull.*, **241** (part 1), 1–27.

Caratini, C., Blasco, F. and **Thanikaimoni, G.** (1973) Relation between the pollen spectra and the vegetation of a South Indian mangrove. *Pollen et Spores*, **XV,** 281–292.

Caratini, C., Thanikaimoni, G. and **Tissot, C.** (1980) Mangroves of India: Palynological study and recent history of the vegetation. *Proc. IV Int. Palynol. Conf., Lucknow (1976–77)*, **3,** 49–59.

Catuneanu, O., Beaymont, C. and **Waschbusch, P.** (1997) Interplay of static loads and subduction dynamics in foreland basins: reciprocal stratigraphies and the 'missing' peripheral bulge. *Geology*, **25,** 1087–1090.

Catuneanu, O., Sweet, A.R. and **Miall, A.D.** (2000) Reciprocal stratigraphy of the Campanian–Paleocene Western Interior of North America. *Sed. Geol.*, **134,** 235–255.

Cerrón-Z., F., Sánchez-F., M.J., Rossel-S., W., Galdos-H., J., Larico-C., W. and **Chacaltana-B., C.** (1999) Geología de los cuadrángulos 1-l, 1-m, 1-n, 1-ñ, 2-m, 2-n, 2-ñ, 3-l, 3-m, 3-n, 3-ñ, 3-o, 4-l, 4-m, 4-n, 4-ñ y 4-o. *Instituto Geológico Minero Metalúrgico, Boletín Serie A: Carta Geológica Nacional, Perú*, **129,** 55–125.

Choi, K.S., Dalrymple, R.W., Chun, S.S. and **Kim, S.-P.** (2004) Sedimentology of modern, inclined heterolithic stratification (IHS) in the macrotidal Han River delta, Korea. *J. Sed. Res.*, **74,** 677–689.

Clifton, H.E. (1982) Estuarine deposits. In: *Sandstone Depositional Environments* (Eds P.A. Scholle and D. Spearing), *AAPG Mem.*, **31,** 179–189.

Clifton, H.E. and **Phillips, R.L.** (1980) Lateral trends and vertical sequences in estuarine sediments, Willapa Bay, Washington. In: *Quaternary Depositional Environments of the Pacific Coast* (Eds M.E. Field, A.H. Bouma, I.P. Colburn, R.G. Douglas and J.C. Ingle), *Pacific Coast Paleogeogr. Symp.*, **4,** 55–71.

Colinvaux, P., De Oliveira, P.E. and **Moreno-Patiño, J.E.** (1999) *Amazon Pollen Manual and Atlas*. Harwood Academic Publishers, Amsterdam, 342 pp.

Cooper, M.A., Addison, F.T., Alvarez, R., Coral, M., Graham, R.H., Hayward, A.B., Howe, S., Martinez, J., Naar, J., Peñas, R., Pulham, A.J. and **Taborda, A.** (1995) Basin development and tectonic history of the Llanos Basin, Eastern Cordillera, and Middle Magdalena Valley, Colombia. *AAPG Bull.*, **79,** 1421–1443.

Dalrymple, R.W. (1984) Morphology and internal structure of sandwaves in the Bay of Fundy. *Sedimentology*, **31,** 365–382.

Dalrymple, R.W. (1992) Tidal depositional systems. In: *Facies Models: Response to Sea Level Change* (Eds R.G. Walker and N.P. James), pp. 195–218. Geological Association of Canada, St John's, Newfoundland.

Dalrymple, R.W., Makino, Y. and **Zaitlin, B.A.** (1991) Temporal and spatial patterns of rhythmite deposition on mud flats in the macrotidal Cobequid Bay-Salmon River estuary, Bay of Fundy, Canada. In: *Clastic Tidal Sedimentology* (Eds D.G. Smith, G.E. Reinson, B.A. Zaitlin and R.A. Rahmani), *CSPG Mem.*, **16,** 137–160.

Dalrymple, R.W., Zaitlin, B.A. and **Boyd, R.** (1992) Estuarine facies models: conceptual basis and stratigraphic implications. *J. Sed. Petrol.*, **62,** 1130–1146.

Dalrymple, R.W., Baker, E.K., Harris, P.T. and **Hughes, M.G.** (2003) Sedimentology and stratigraphy of a tide-dominated, foreland-basin delta (Fly River, Papua New Guinea). In: *Tropical Deltas of Southeast Asia – Sedimentology, Stratigraphy, and Petroleum Geology* (Eds F.H. Sidi, D. Num-

medal, P. Imbert, H. Darman and H.W. Posamentieir), *SEPM Spec. Publ.*, **76,** 147–173.

DeCelles, P.G. and **Giles, K.A.** (1996) Foreland basin systems. *Basin Res.*, **8,** 105–123.

Díaz de Gamero, M.L. (1996) The changing course of the Orinoco River during the Neogene: a review. *Palaeogeogr. Palaeoclimatol. Palaeoecol.*, **123,** 385–402.

van Den Berg, J.H. (1981) Rhythmic seasonal layering in a mesotidal channel fill sequence, Oosterschelde Mouth, the Netherlands. In: *Holocene Marine Sedimentation in the North Sea Basin: An Introduction* (Ed. S.-D. Nio), *Spec. Publ. Int. Assoc. Sediment.*, **5,** 147–159.

Fan, D. and **Li, C.** (2002) Rhytmic deposition on mudflats in the mesotidal Changjiang Estuary, China. *J. Sed. Res.*, **72,** 543–551.

Frey, R.W. and **Bromley, R.G.** (1985) Ichnology of American chalks: the Selma Group (Upper Cretaceous), western Alabama. *Can. J. Earth Sci.*, **22,** 801–828.

Fu, S. and **Werner, F.** (2000) Distribution, ecology and taphonomy of the organism trace, *Scolicia*, in Northeast Atlantic deep-sea sediments. *Palaeogeogr. Palaeoclimatol. Palaeoecol.*, **156,** 289–300.

Germeraad, J.H., Hopping, C.A. and **Muller, J.** (1968) Palynology of tertiary sediments from tropical areas. *Rev. Palaeobot. Palynol.*, **6,** 189–348.

Gil, W. (2001) *Evolution latérale de la déformation d'un front orogénique: Exemples des bassins subandins entre 0° et 16°S*. PhD Thesis, Université Paul Sabatier, Toulouse, France, 156 pp.

Gingras, M.K., Pemberton, S.G. and **Saunders, T.** (1999) The ichnology of modern and Pleistocene brackish-water deposits at Willapa Bay, Washington: variability in estuarine settings. *Palaios*, **14,** 352–374.

Gingras, M.K., Hubbard, S.M., Pemberton, S.G. and **Saunders, T.** (2000) The significance of Pleistocene *Psilonichnus* at Willapa Bay, Washington. *Palaios*, **15,** 142–151.

Gingras, M.K., Räsänen, M. and **Ranzi, A.** (2002a) The significance of bioturbated inclined heterolithic stratification in the southern part of the Miocene Solimões Formation, Rio Acre, Amazonia Brazil. *Palaios*, **17,** 591–601.

Gingras, M.K., Räsänen, M.E., Pemberton, G. and **Romero, L.** (2002b) Ichnology and sedimentology reveal depositional characteristics of bay margin parasequences in the Miocene Amazonian Foreland Basin. *J. Sed. Res.*, **72,** 871–883.

Guerrero, J. (1997) Stratigraphy, sedimentary environments, and the Miocene uplift of the Colombian Andes. In: *Vertebrate Paleontology in the Neotropics: The Miocene Fauna of La Venta, Colombia* (Eds R.F. Kay, R.H. Madden, R.L. Cifelli and J.J. Flynn), pp. 15–43. Smithsonian Institution Press, Washington, DC.

Hermoza, W., Brusset, S., Baby, P., Gil, W., Roddaz, M., Guerrero, N. and **Bolaños, M.** (2005) The Huallaga foreland basin evolution: Thrust propagation in a deltaic environment, northern Peruvian Andes. *J. South Am. Earth Sci.*, **19,** 21–34.

Hoorn, C. (1993a) Marine incursions and the influence of Andean tectonics on the Miocene depositional history of northwestern Amazonia: results of a palynostratigraphic study. *Palaeogeogr. Palaeoclimatol. Palaeoecol.*, **105,** 267–309.

Hoorn, C. (1993b) Geología del Nororiente de la Amazonia Peruana: la formación Pebas. In: *Amazonia Peruana – Vegetación húmeda tropical en el llano subandino* (Eds R. Kalliola, M. Puhakka and W. Danjoy), pp. 69–85. Paut and Onern, Jyväskylä.

Hoorn, C. (1994a) Fluvial palaeoenvironments in the intracratonic Amazonas Basin (Early Miocene–early Middle Miocene, Colombia). *Palaeogeogr. Palaeoclimatol. Palaeoecol.*, **109,** 1–54.

Hoorn, C. (1994b) An environmental reconstruction of the palaeo-Amazon River system (Middle–Late Miocene, NW Amazonia). *Palaeogeogr. Palaeoclimatol. Palaeoecol.*, **112,** 187–238.

Hoorn, C. (1994c) *Miocene palynostratigraphy and paleoenvironments of northwestern Amazõnia: evidence for marine incursions and the influence of Andean tectonics*. PhD Thesis, University of Amsterdam, Amsterdam The Netherland, 156 pp.

Hoorn, C. and **Vonhof, H.** (2006) Neogene Amazonia: introduction to the special issue. *J. South Am. Earth Sci.*, **21,** 1–4, doi: 10.1016/j.jsames.2005.09.002.

Hoorn, C., Guerrero, J., Sarmiento, G.A. and **Lorente, M.A.** (1995) Andean tectonics as a cause for changing drainage patterns in Miocene northern South America. *Geology*, **23,** 237–240.

Horton, B.K. and **DeCelles, P.G.** (1997) The modern foreland basin system adjacent to the Central Andes. *Geology*, **25,** 895–898.

Hovikoski, J., Räsänen, M., Gingras, M., Roddaz, M., Brusset, S., Hermoza, W. and **Romero Pittman, L.** (2005) Miocene semidiurnal tidal rhythmites in Madre de Dios, Peru. *Geology*, **33,** 177–180.

Hulka, C., Gräfe, K.-U., Sames, B., Uba, C.E. and **Heubeck, C.** (2006) Depositional setting of the middle to late Miocene Yecua Formation of the Chaco Foreland Basin, southern Bolivia. In: *New contributions on Neogene geography and depositional environments in Amazonia* (Eds C. Hoorn and H. Vonhof). *J. South Am. Earth Sci.*, **21,** 135–150, doi: 10.1016/j.jsames-2005.08.003.

Hungerbühler, D., Steinmann, M., Winkler, W., Seward, D., Egüez, A., Peterson, D.E., Helg, U. and **Hammer, C.** (2002) Neogene stratigraphy and Andean geodynamics of southern Ecuador. *Earth-Sci. Rev.*, **57,** 75–124.

Jacques, J.M. (2003a) A tectonostratigraphic synthesis of the Sub-Andean basins: implications for the geotectonic segmentation of the Andean Belt. *J. Geol. Soc. London*, **160,** 687–701.

Jacques, J.M. (2003b) A tectonostratigraphic synthesis of the Sub-Andean basins: inferences on the position of South American intraplate accomodation zones and their control on South Atlantic opening. *J. Geol. Soc. London*, **160,** 703–717.

Jordan, T.E., Isacks, B.L., Allmendinger, R.W., Brewer, J.A., Ramos, V.A. and **Ando, C.J.** (1983) Andean tectonics related to geometry of subducted Nazca plate. *Geological Society of America Bulletin*, **94,** 341–361.

Kaandorp, R.J.G., Vonhof, H.B., Wesselingh, F.P., Romero Pittman, L., Kroon, D. and **van Hinte, J.E.** (2005) Seasonal Amazonian rainfall variation in the Miocene Climate Optimum. *Palaeogeogr. Palaeoclimatol. Palaeoecol.*, **221,** 1–6.

Le Bot, S. and **Trentesaux, A.** (2004) Types of internal structure and external morphology of submarine dunes under the influence of tide- and wind-driven processes (Dover Strait, northern France). *Mar. Geol.*, **211,** 143–168.

Leite, F.P.R. (1997) *Palinofloras Neógenas da Formação Pirabas e Grupo Barreiras, área litorãnea nordeste do Estado*

do Pará, Brasil. MSc Thesis, Universidade de São Paulo, Brazil, 111 pp.

Lorente, M.A. (1986) *Palynology and Palynofacies of the Upper Tertiary in Venezuela*. PhD Thesis, University of Amsterdam, Amsterdam, 222 pp.

Lovejoy, N.R., Bermingham, E. and **Martin, A.P.** (1998) Marine incursions into South America. *Nature*, **396,** 421–422.

Lundberg, J.G., Marshall, L.G., Guerrero, J., Horton, B., Malabarba, M.C.S.L. and **Wesselingh, F.** (1998) The stage of Neotropical fish diversification: a history of tropical South American rivers. In: *Phylogeny and Classification of Neotropical Fishes* (Eds L.R. Malabarba, R.E. Reis, R.P. Vari, Z.M. Lucena and C.A.S. Lucena), pp. 13–48. Edipucrs, Porto Alegre, Brazil.

Maia, R.G., Godoy, H.K., Yamaguti, H.S., De Moura, P.A., Da Costa, F.S., De Holanda, M.A. and **Costa, J.** (1977) Projeto de Carvâo no Alto Solimões. *Relatório Final*, **1,** CPRM-DNPM, pp. 61–92. and fig. 6.

Marengo, H.G. (2000) Rasgos micropaleontológicos de los depósitos de la transgresión Entrerriense-Paranense en la Cuenca Chaco-Paranense y Noroeste Argentino, República Argentina. In: *El Neógeno de Argentina* (Eds F.G. Aceñolaza and R. Herbst), pp. 29–45. INSUGEO, Tucumán, Argentina.

Marshall, L.G. and **Sempere, T.** (1991) The Eocene to Pleistocene vertebrates of Bolivia and their stratigraphic context: a review. In: *Fósiles y facies de Bolivia – Vol I Vertebrados* (Ed. R. Suárez-Soruco), pp. 631–652. Revista Técnica de Ya cimientos Petrolíferos Fiscales Bolivianos, vol. no. 1, La Paz, Bolivia.

Marshall, L.G., Sempere, T. and **Gayet, M.** (1993) The Petaca (Late Oligocene-Middle Miocene) and Yecua (Late Miocene) Formations of the Subandean-Chaco Basin, Bolivia, and their tectonic significance. *Docum. Lab. Géol. Lyon*, **125,** 291–301.

Martínez, S. and **del Río, C.J.** (2002) Late Miocene molluscs from the southwestern Atlantic Ocean (Argentina and Uruguay): a palaeobiogeographic analysis. *Palaeogeogr. Palaeoclimatol. Palaeoecol.*, **188,** 167–187.

Martínez-V., W., Morales, R.M., Díaz, H.G., Milla, S.D., Montoya, P.C., Huayhua, R.J., Romero, P.L. and **Raymundo, S.T.** (1999) Geología de los cuadrángulos de 5-n, 5-ñ, 5-o, 6-n, 6-ñ, 6-o, 7-n, 7-ñ, 7-o, 8-n, 8-ñ, 8-o, 9-n, 9-ñ, 9-o, 10-n, 10-ñ y 10-o. *Instituto Geológico Minero Metalúrgico, Boletín Serie A: Carta Geológica Nacional (Perú)*, **131,** 1–8, 51–169, 191–193,

McIlroy, D. (2004) Ichnofabrics and sedimentary facies of a tide-dominated delta: Jurassic Ile Formation of Kristin Field, Haltenbanken, Offshore Mid-Norway. In: *The Application of Ichnology to Palaeoenvironmental and Stratigraphic Analysis* (Ed. D. McIlroy), *Geol. Soc., London, Spec. Publ.*, **228,** 237–272.

Mörner, N.-A., Rossetti, D. and **Toledo, P.M.** (2001) The Amazonian rainforest only some 6–5 million years old. In: *Diversidade biológica e cultural da Amazônia* (Eds I.C.G. Vieira, J.M.C. Silva, D.C. Oren and M.A. D'Incao), pp. 3–18. Museu Paraense Emílio Goeldi, Belém – Pará, Brazil.

Muller, J., Di Giacomo, E. and **Van Erve, A.W.** (1987) A palynological zonation for the Cretaceous, Tertiary, and Quaternary of Northern South America. *Am. Assoc. Stratigraph. Palynol. Found. Contrib. Ser.*, **19,** 7–76.

Nio, S.-D. and **Yang, C.S.** (1991) Diagnostic attributes of clastic tidal deposits: a review. In: *Clastic Tidal Sedimentology* (Eds D.G. Smith, G.E. Reinson, B.A. Zaitlin and R.A. Rahmani), *Can. Soc. Petrol. Geol. Mem.*, **16,** 3–28.

Nuttall, C.P. (1990) A review of the Tertiary non-marine molluscan faunas of the Pebasian and other inland basins of north-western South America. *Bull. Br. Mus. Nat. Hist. (Geol.)*, **45,** 165–371.

Pemberton, S.G. and **Frey, R.W.** (1982) Trace fossil nomenclature and the *Planolites–Palaeophycus* dilemma. *J. Paleontol.*, **56,** 843–881.

Pemberton, S.G., Flach, P.D. and **Mossop, G.D.** (1982) Trace fossils from the Athabasca Oil Sands, Alberta, Canada. *Science*, **217,** 825–827.

Pemberton, S.G., MacEachern, J.A. and **Frey, R.W.** (1992) Trace fossil facies models: Environmental and allostratigraphic significance. In: *Facies Models: Response to Sea Level Change* (Eds R.G. Walker and N.P. James), pp. 47–72. Geological Association of Canada, St John's, Newfoundland.

Plaziat, J.-C. (1995) Modern and fossil mangroves and mangals: their climatic and biogeographic variability. In: *Marine Palaeoenvironmental Analysis from Fossils* (Eds D.W.J. Bosence and P.A. Allison), *Geol. Soc. Spec. Publ.*, **83,** 73–96.

Plaziat, J.-C. and **Mahmoudi, M.** (1988) Trace fossils attributed to burrowing echinoids: a revision including new ichnogenus and ichnospecies. *Geobios*, **21,** 209–233.

Plummer, P.S. and **Gostin, V.A.** (1981) Shrinkage cracks: desiccation or synaeresis. *J. Sed. Petrol.*, **51,** 1147–1156.

Pratt, B.R. (1998) Syneresis cracks: subaqueous shrinkage in argillaceous sediments caused by earthquake-induced dewatering. *Sed. Geol.*, **117,** 1–10.

Räsänen, M.E., Linna, A.M., Santos, J.C.R. and **Negri, F.R.** (1995) Late Miocene tidal deposits in the Amazonian foreland basin. *Science*, **269,** 386–390.

Räsänen, M., Linna, A., Irion, G., Rebata-H, L.A., Wesselingh, F. and **Vargas, R.** (1998) Geología y geoformas de la zona de Iquitos. In: *Geoecología y desarrollo Amazónico. Estudio integrado en la zona de Iquitos, Perú* (Eds R. Kalliola and S. Flores), *Annales Universitatis Turkuensis Ser. A II*, **114,** 59–137.

Rebata-H., L.A. (1997) *Description of Neogene–Quaternary tide and wave-influenced estuary-sediments along Nauta–Iquitos Road, km 0–15, Loreto-Peru, NW Amazonia*. Master's Thesis, University of Turku, Finland, 105 pp.

Rebata-H., L.A., Räsänen, M.E., Gingras, M.K., Vieira, V. Jr., Barberi, M. and **Irion, G.** (2006) Sedimentology and ichnology of tide-influenced Late Miocene successions in Western Amazonia: the gradational transition between the Pebas and Nauta formations. In: *New contributions on Neogene geography and depositional environments in Amazonia* (Eds C. Hoorn and H. Vonhof). *J. South Am. Earth Sci.*, **21,** 96–119, doi: 10.1016/j.jsames.2005.07.011.

van Reeuwijk, L.P. (ed.) (1992) *Procedures for Soil Analysis*, 3rd edn. pp. 3-1–3-2. ISRIC, Technical paper 9, Wageningen, The Netherlands.

Reineck, H.-E. and **Singh, I.** (1986) *Depositional Sedimentary Environments: With Reference to Terrigenous Clastics*. 2nd, revised and updated edn. Corrected 2nd printing. pp. 95–131, 382–423. Springer Verlag, Berlin.

Reineck, H.-E. and **Wunderlich, F.** (1968) Classification and origin of flaser and lenticular bedding. *Sedimentology*, **11,** 99–104.

Roddaz, M., Baby, P., Brusset, S., Hermoza, W. and **Darrozes, J.M.** (2005) Forebulge dynamics and environmental control in Western Amazonia: The case study of the Arch of Iquitos (Peru). *Tectonophysics*, **399,** 87–108.

Rossetti, D.F. (2001) Late Cenozoic sedimentary evolution in northeastern Pará, Brazil, within the context of sea level changes. *J. South Am. Earth Sci.*, **14,** 77–89.

Rossetti, D.F. and **Santos, A.E. Jr.** (2003) Events of sediment deformation and mass failure in Upper Cretaceous estuarine deposits (Cametá Basin, northern Brazil) as evidence for seismic activity. *Sed. Geol.*, **161,** 107–130.

Rossetti, D.F., Toledo, P.M. and **Góes, A.M.** (2005) New geological framework for Western Amazonia (Brazil) and implications for biogeography and evolution. *Quatern. Res.*, **63,** 78–89.

Rull, V. (2001) A quantitative palynological record from the Early Miocene of Western Venezuela, with emphasis on mangroves. *Palynology*, **25,** 109–126.

Sánchez-F., A., Chira, F.J., Romero, F.D., De la Cruz, W.J., Herrera, T.I., Cervante, G.J., Monge, M.R., Valencia, M.M. and **Cuba, M.A.** (1999) *Geología de los cuadrángulos 4-p, 5-p, 5-q, 5-r, 6-p, 6-q, 6-r, 7-p, 7-q, 7-r, 8-p, 8-q, 8-r, 9-p, 9-q, 9-r, 10-p, 10-q y 10-r.* Instituto Geológico Minero Metalúrgico, Boletín Serie A Carta Geológica Nacional, Perú, **132,** 1–12, 91–179, 261–264.

Seilacher, A. (1963) Lebensspurren und Salinitätsfazies. *Forstschr. Geol. Rheinld. U. Westf.*, **10,** 81–94.

Seilacher, A. (1967) Bathymetry of trace fossils. *Mar. Geol.*, **5,** 413–428.

Siiro, P. (2002) Characteristic grain-size distribution patterns of tidally-influenced coastal plain estuarine sediments based on comparative studies of the Cretaceous McMurray Formation in Alberta, Canada and the Miocene Pebas/Solimões formation in Western Amazonia, Peru and Brazil. Licentiate Thesis, University of Turku, Finland, pp. 10–11.

Smith, A.B. and **Crimes, T.P.** (1983) Traced fossils formed by heart urchins – a study of *Scolicia* and related traces. *Lethaia*, **16,** 79–92.

Steinmann, M., Hungerbühler, D., Seward, D. and **Winkler, W.** (1999) Neogene tectonic evolution and exhumation of the southern Ecuadorian Andes: a combined stratigraphy and fission-track approach. *Tectonophysics*, **307,** 255–276.

Tanner, P.W.G. (1998) Interstratal dewatering origin for polygonal patterns of sand-filled cracks: a case study from late Proterozoic metasediments of Islay, Scotland. *Sedimentology*, **45,** 71–89.

Terwindt, J.H.J. (1975) Sequences in inshore subtidal deposits. In: *Tidal Deposits: A Casebook of Recent Examples and Fossil Counterparts* (Ed. R.N. Ginsburg), Springer-Verlag, New York.

Terwindt, J.H.J. and **Breusers, N.H.C.** (1972) Experiments on the origin of flaser, lenticular and sand-clay alternating bedding. *Sedimentology*, **19,** 85–98.

Tessier, B. (1998) Tidal cycles: annual versus semi-lunar records. In: *Tidalites: Processes and Products* (Eds C.R. Alexander, R.A. Davis and V.J. Henry), *SEPM Spec. Publ.*, **61,** 71–74.

Thomas, R.G., Smith, D.G., Wood, J.M., Visser, J., Calverly-Range, E.A. and **Koster, E.H.** (1987) Inclined heterolithic stratification: terminology, description, interpretation, and significance. *Sed. Geol.*, **53,** 123–179.

Thunell, R., Rio, D., Sprovieri, R. and **Raffi, I.** (1991) Limestone-marl couplets: origin of the Early Pliocene Trubi Marls in Calabria, Southern Italy. *J. Sed. Res.*, **61,** 1109–1122.

Vonhof, H., Wesselingh, F. and **Ganssen, G.** (1998) Reconstruction of the Miocene Western Amazonian aquatic system using molluscan isotopic signatures. *Palaeogeogr. Palaeoclimatol. Palaeoecol.*, **141,** 85–93.

Vonhof, H.B., Wesselingh, F.P., Kaandorp, R.J.G., Davies, G.R., van Hinte, J.E., Guerrero, J., Räsänen, M., Romero-Pittman, L. and **Ranzi, A.** (2003) Paleogeography of Miocene Western Amazonia: isotopic composition of molluscan shells constrains the influence of marine incursions. *GSA Bull.*, **115,** 983–993.

Webb, S.D. (1995) Biological Implications of the Middle Miocene Amazon Seaway. *Science*, **269,** 361–362.

Wesselingh, F.P., Räsänen, M.E., Irion, G., Vonhof, H.B., Kaandorp, R., Renema, W., Romero Pittman, L. and **Gingras, M.** (2002) Lake Pebas: a palaeoecological reconstruction of a Miocene, long-lived lake complex in western Amazonia. *Cainozoic Res.*, **1** (1–2) (2001), 35–81.

Whatley, R., Muñoz-Torres, F. and **Van Harten, D.** (1998) The ostracoda of an isolated Neogene saline lake in the Western Amazon basin. In: *Proceedings of the Third European Symposium on Ostracoda: What about Ostracoda!, Bierville, 1996. Bull. Centre Rech. Elf. Explor. Prod. Mém.*, **20,** 231–245.

Yamamoto, I.T. (1995) *Palinologia das bacias tafrogênicas do Sudeste (Bacias de Taubaté, São Paulo e Resende): Análise bioestratigráfica integrada e interpretação paleoambiental.* MSc Thesis, Universidade Estadual Paulista, Brazil, 217 pp.

Ybert, J.P., Salgado-Labouriau, M.L., Barth, M.O., Lorscheitter, M.L., Barros, M.A., Chaves, S.A.M., Luz, C.F.P., Barberi-Ribeiro, M., Scheel, R. and **Ferraz-Vicentini, K.R.** (1992) Sugestões para padronização da metodologia empregada em estudos palinológicos do Quaternário. *IG, São Paulo*, **13,** 47–49.

Zonneveld, J.-P., Gingras, M.K. and **Pemberton, S.G.** (2001) Trace fossil assemblages in a Middle Triassic mixed siliciclastic-carbonate marginal marine depositional system, British Columbia. *Palaeogeogr. Palaeoclimatol. Palaeoecol.*, **166,** 249–276.

Manuscript received 14 November 2003; revision accepted 30 August 2005